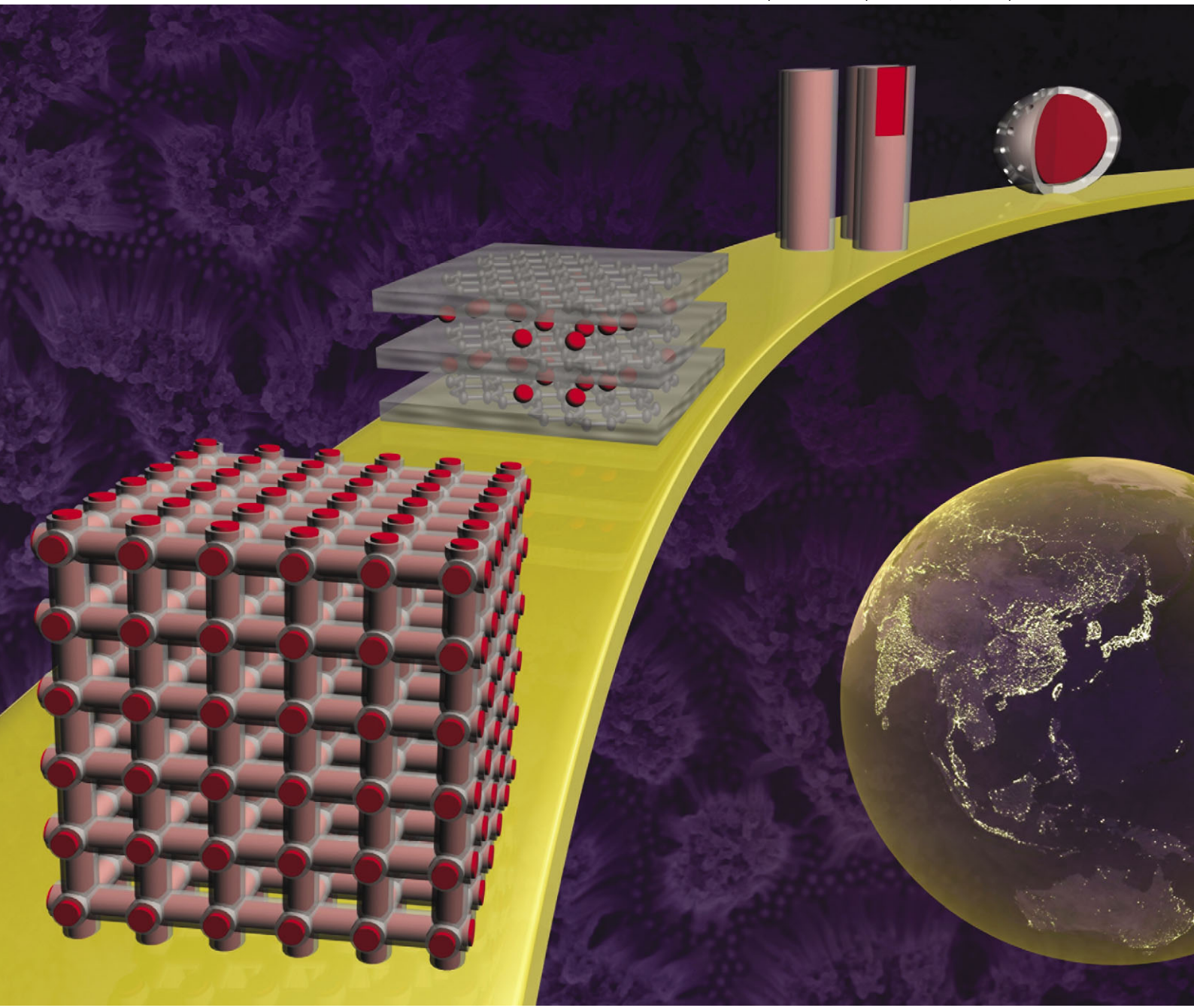


# ChemComm

Chemical Communications

[www.rsc.org/chemcomm](http://www.rsc.org/chemcomm)

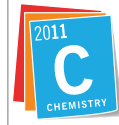
Volume 47 | Number 5 | 7 February 2011 | Pages 1353–1636



ISSN 1359-7345

RSC Publishing

**FEATURE ARTICLE**  
Sang Bok Lee *et al.*  
Heterogeneous nanostructured  
electrode materials for  
electrochemical energy storage



International Year of  
**CHEMISTRY**  
**2011**



1359-7345(2011)47:5;1-B

# Heterogeneous nanostructured electrode materials for electrochemical energy storage

Ran Liu,<sup>†[a](#)</sup> Jonathon Duay<sup>a</sup> and Sang Bok Lee<sup>\*ab</sup>

Received 10th August 2010, Accepted 22nd October 2010

DOI: 10.1039/c0cc03158e

In order to fulfil the future requirements of electrochemical energy storage, such as high energy density at high power demands, heterogeneous nanostructured materials are currently studied as promising electrode materials due to their synergic properties, which arise from integrating multi-nanocomponents, each tailored to address a different demand (*e.g.*, high energy density, high conductivity, and excellent mechanical stability). In this article, we discuss these heterogeneous nanomaterials based on their structural complexity: zero-dimensional (0-D) (*e.g.* core–shell nanoparticles), one-dimensional (1-D) (*e.g.* coaxial nanowires), two-dimensional (2-D) (*e.g.* graphene based composites), three-dimensional (3-D) (*e.g.* mesoporous carbon based composites) and the even more complex hierarchical 3-D nanostructured networks. This review tends to focus more on ordered arrays of 1-D heterogeneous nanomaterials due to their unique merits. Examples of different types of structures are listed and their advantages and disadvantages are compared. Finally a future 3-D heterogeneous nanostructure is proposed, which may set a goal toward developing ideal nano-architected electrodes for future electrochemical energy storage devices.

## Introduction

One of the major challenges facing researchers today is to provide highly efficient, low cost, and environmentally benign electrical energy storage (EES) devices to address the problems of climate change, the impending exhaustion of fossils fuels

and the dire need for efficient storage of energy produced by solar and wind power.<sup>1–19</sup> Lithium ion batteries<sup>1,2,4,6,8–10,14,15,17</sup> and supercapacitors<sup>1,13,16,18,19</sup> are at the frontier of this research effort, as they play important roles in our daily lives by powering numerous portable consumer electronic devices (*e.g.*, cell phones, PDAs, laptops) and even current plug-in hybrid electric vehicles (PHEVs).

A typical commercial lithium–ion battery is comprised of a graphite negative electrode (anode), a non-aqueous liquid electrolyte, and a positive electrode (cathode) formed from layered LiCoO<sub>2</sub> (Scheme 1). On charging, lithium ions are extracted from the layered LiCoO<sub>2</sub> intercalation host, pass through the electrolyte, and intercalate between the graphite

<sup>a</sup> Department of Chemistry and Biochemistry, University of Maryland, College Park, MD 20742, USA. E-mail: slee@umd.edu; Fax: +1 301 314 9121; Tel: +1 301 405 7906

<sup>b</sup> Graduate School of Nanoscience and Technology (WCU), Korea Advanced Institute of Science and Technology, Daejeon 305-701, Korea

† Present Address: Department of Chemistry, Pennsylvania State University, State College, PA 16802, USA.



Ran Liu

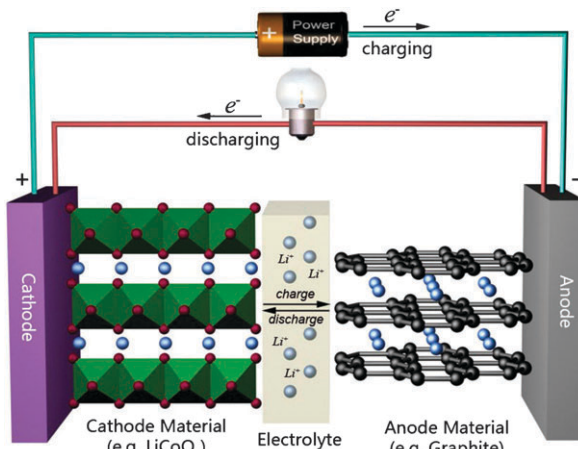
Ran Liu was born in Tianjin, China. He earned his BE in Chemical Engineering from Jilin University in 2002, his MSc in chemistry from the University of New Orleans in 2004, and his PhD in chemistry from the University of Maryland, College Park. He is currently at Pennsylvania State University pursuing his postdoctoral studies under Prof. Ayusman Sen. His research interests have included the template synthesis of heterogeneous nanomaterials

and their applications, with an emphasis on developing new approaches to synthesize electrode materials for electrochemical energy storage devices, such as supercapacitors and lithium–ion batteries.



Jonathon Duay

Jonathon Duay was born in Worland, Wyoming (US). He received his BSc in Chemistry from Weber State University (Ogden, UT) in 2008. He is currently a PhD Chemistry student at the University of Maryland, College Park in Professor Sang Bok Lee's group. His research interests include the synthesis of one-dimensional heterogeneous nanowire arrays for high power energy storage applications.

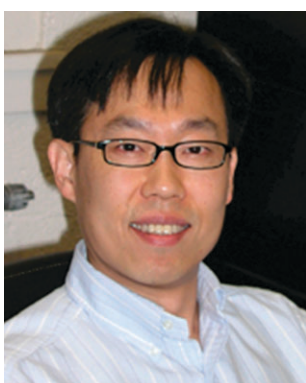


**Scheme 1** Typical commercial Li-ion battery showcasing the charge/discharge intercalation mechanism.

layers in the anode. Discharge is the reverse of this process. The electrons, of course, pass through the external circuit.

Heavily researched anode materials include carbon,<sup>21–23</sup> silicon,<sup>24</sup> titanium dioxide,<sup>25</sup> and tin<sup>26</sup> among others, while typically researched cathode materials include LiMn<sub>2</sub>O<sub>4</sub>,<sup>26,27</sup> V<sub>2</sub>O<sub>5</sub>,<sup>28</sup> and LiFePO<sub>4</sub><sup>14,29,30</sup> to name a few. These materials are rated by their specific (gravimetric) capacity (mAh/g), calculated from their charge/discharge graphs (galvanostatic voltammograms), as well as the degree that this capacity changes upon cycling and at high power demands. This capacity highlights how much charge can be stored in a given mass of material before the potential exceeds its electrochemically reversible window. However, when one compares these capacities from one material to another they must take into account the potential window, electrolyte used, composition of the electrode (additives), charge/discharge efficiency as well as their volumetric and areal capacities all of which may or may not be included by the authors.

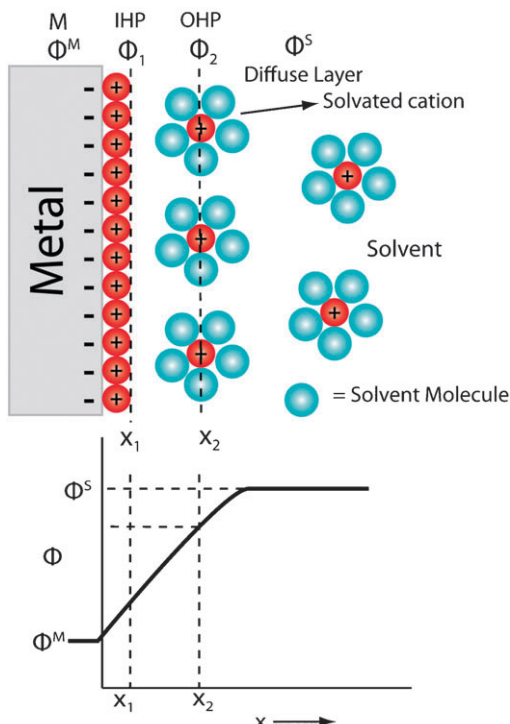
Supercapacitors are capacitors that contain an electrolyte solution in place of a dielectric layer. They are called “super” because of their extraordinarily high energy density when



**Sang Bok Lee**

*Sang Bok Lee is an Associate Professor at the Department of Chemistry and Biochemistry and Associate Director of the DOE-EFRC (Energy Frontier Research Center), University of Maryland (UMD), College Park, MD, USA and also holds a WCU professorship at KAIST in Korea. He received his B.S., M.S., and PhD (1997) in Chemistry from Seoul National University, Korea. His research focuses on the fundamentals of synthesis and control of heterogeneous nanowire structures and fast electrochemistry of nanomaterials from high power energy storage to electronics to nanomedicine.*

geneous nanowire structures and fast electrochemistry of nanomaterials from high power energy storage to electronics to nanomedicine.



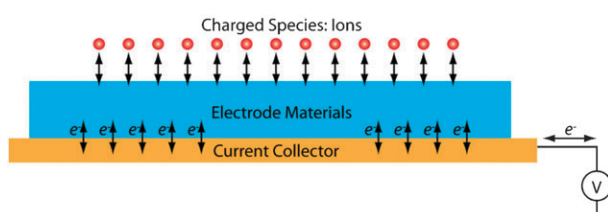
**Scheme 2** Illustration showing the double layer formation of a typical EDLC electrode with IHP and OHP standing for the inner Helmholtz plane and outer Helmholtz plane, respectively. The graph represents the potential gradient across the double layer with  $\Phi^S$  and  $\Phi^M$  corresponding to the potential of the electrolyte solution and the potential of the electrode metal, respectively.

compared to traditional electrolytic or electrostatic capacitors. These devices can be composed using the same material for the cathode and anode as in a symmetric device or use different materials for each as in an asymmetric device.

Supercapacitors can be divided into two separate types depending on their charge storage mechanism: Electrochemical Double Layer Capacitors (EDLCs) and Pseudocapacitors.

EDLCs store their charge in the double layer that forms between the electrode material and the electrolyte upon charging (Scheme 2). Therefore, traditional materials for these devices have included high surface area carbons<sup>16</sup> and nanostructured conductive substrates such as TiO<sub>2</sub> nanotubes.<sup>31</sup>

Pseudocapacitors do not rely on the traditional charge separation mechanism that is typical of a capacitor. They rely on a fast surface or near-surface faradaic charge-transfer mechanism which gives them their “pseudo”-capacitive behavior (Scheme 3). Thus, their electrochemical properties are nearly



**Scheme 3** Charge storage mechanism of pseudocapacitive materials showing the surface charge transfer reaction.

identical with those of traditional capacitors. Transition metal oxides such as RuO<sub>2</sub>,<sup>32,33</sup> Fe<sub>3</sub>O<sub>4</sub>,<sup>34,35</sup> and MnO<sub>2</sub><sup>36</sup> along with conductive polymers<sup>1,37</sup> such as polypyrrole, polyaniline, and polythiophene are the typical materials used for these devices.

Both EDLC and pseudocapacitive materials are rated by their specific capacitance (F/g), obtained from their cyclic voltammetry (CV) or charge/discharge graphs, as well as the extent that this capacitance fades upon cycling and at high power demands. As with specific capacity, specific capacitance highlights how much charge can be stored in a given mass of material before the potential exceeds its electrochemically reversible window; however, for capacitors this charge is ideally evenly distributed along the electrochemically reversible voltage window thus capacitance is just the capacity in units of coulombs divided by the potential window as a farad (F) is equal to the charge divided by the voltage. As with battery material ratings (specific capacity), one must take into account a variety of factors before comparing these numbers.

The future will require these battery and supercapacitor devices to be able to achieve extraordinarily high energy densities at high rate capabilities.<sup>8,11,17,29,38,39</sup> These stipulations will necessitate revolutionary advances for these devices such as using innovative electrode materials with architecturally tailored nanostructures.

Nanostructured electrode materials have great advantages over their bulk counterparts in fulfilling the above mentioned goals. Due to the small size of the material, lithium ions have shorter path lengths resulting in higher lithium ion capacities at high charge/discharge rates. Also, their small size can buffer any stresses associated with the crystal unit cell expansion/contraction during the lithium ion intercalation/deintercalation process reducing capacity losses associated with the material breaking away into the electrolyte. Additionally, the interface between the electrode material and electrolyte is enhanced resulting in a higher lithium ion flux when compared to the bulk.<sup>3–5,7,9–11,13,40</sup>

However, nanomaterials, especially single-phased nanomaterials, are certainly not an elixir, and may not be able to fulfill the requirements of future EES devices because of some of their intrinsic material properties such as low conductivities,<sup>29,41</sup> slow kinetics (low energy densities at high charge/discharge rates),<sup>27,34</sup> poor cyclability,<sup>42</sup> and weak mechanical stabilities<sup>22</sup> which can not be simply altered and enhanced by just transforming them into nanomaterials. Moreover, without some surface protection, nanomaterials may have significant side reactions with the electrolyte and may agglomerate due to their high surface area and high surface energy, which may lead to a high level of irreversibility and thus poor cycle life.<sup>42,43</sup>

In order to transcend the above limitations of using single component nanostructured electrode materials, heterogeneous nanostructured materials with multi-nanocomponents, each tailored to address a different demand (*e.g.*, high energy density, high conductivity, and excellent mechanical stability) have been synthesized.<sup>34,41,44–47</sup> The resulting materials have been shown to exhibit synergic properties by integrating the individual components, realizing the full potential of

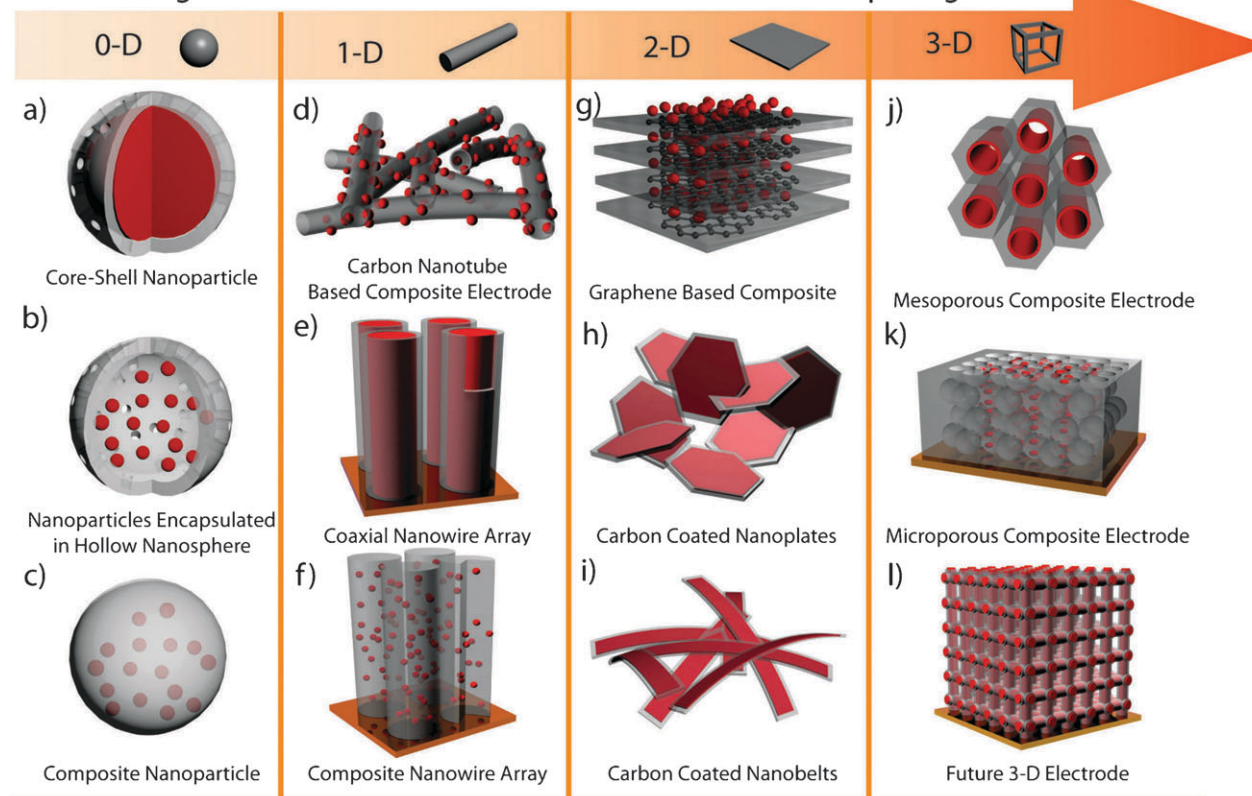
the materials in terms of performance (*e.g.* high energy density and high rate capabilities).<sup>34,41,44–52</sup> For example, Core–shell nanoparticles composed of LiFePO<sub>4</sub> and carbon have been reported to yield enhanced conductivities resulting in fast charge/discharge rates.<sup>52</sup> Coaxial nanowires comprised of an MnO<sub>2</sub> core with a PEDOT shell has been prepared by our group. The synergic properties and functionalities of these two materials enable this composite material to exhibit a high energy density at high power densities.<sup>46</sup>

While there are quite a few excellent reviews on the application of nanostructured materials for lithium ion batteries and supercapacitors in the literature,<sup>3–5,7,9–11,13,40</sup> these tend to focus on the single-phase nanomaterials. In this article, we concentrate on the recent progress of using heterogeneous nanostructured electrode materials for use in electrochemical energy storage devices. The success of applying heterogeneous nanostructured materials in energy storage hinges on the following factors in particular: (1) selecting a proper combination of different materials; (2) designing and optimizing the heterogeneous nanostructure (*e.g.*, coaxial nanowires,<sup>34,46</sup> core–shell nanoparticles),<sup>51,52</sup> and (3) employing proper methods to synthesize or to assemble the nanocomponents into the desired nanostructures.

To design and optimize heterogeneous nanostructures both theoretically and experimentally is of particular importance, since each of the respective material's properties can be dramatically enhanced if the appropriate nanostructure is chosen. Thus, in the following discussion, we will classify the heterogeneous nanomaterials into 4 major categories based on the their structural complexity, *i.e.* from simplest 0-dimensional (0-D) to the most complex 3-dimensional (3-D) nanostructures. (See Scheme 4). Some of these major categories are split into sub categories based on the different ways of combining the materials into their sub-level nanostructures. For example, core–shell nanoparticles are composed of a spherical core and a distinctive shell while composite nanoparticles are formed when different materials are uniformly mixed and confined into nanoscaled spherical shapes with each component maintaining its distinctive morphology and properties.

Accordingly, this review is structured as follows: First, 0-D heterostructured nanomaterials such as core–shell nanoparticles and nanoparticles loaded with nanospheres are discussed in section 2. Following that, 1-D nanostructures such as coaxial nanowires and surface coated carbon nanotubes will be the focus of section 3. This section will be the main focal point of this review because 1-D nanomaterials, especially ordered arrays of 1-D nanomaterials, have recently received special attentions due to their unique advantages.<sup>22,27,32,34,46,47,53–66</sup> The recent work by our group is also summarized in this section. Section 4 will sum up the 2-D nanostructures such as graphene composite nanomaterials. The most complex 3-D nanostructured network, such as hierarchy networks, ordered mesoporous structures and even the future 3-D architected nanomaterials will be the topic for section 5. Finally, A recap of this review and the future outlook for these heterogeneous nanostructures is given in section 6.

## Heterogeneous Nanostructured Materials with Different Morphologies



**Scheme 4** Different heterogeneous nanostructured materials based on structural complexity.

## 2. Zero-dimensional (0-D) heterogeneous nanostructures

The 0-D nanostructure usually refers to spherically-shaped nanoparticles with diameters ranging from a few to tens of nanometers. Metal oxide, metal phosphide, and oxy salt nanoparticles have been widely investigated as electrode materials for lithium ion batteries.<sup>67–69</sup> Due to their small dimensions, the lithium ion diffusion path is reduced and the collective electrode stress caused by Li insertion/removal can be lowered.

Therefore, an improved rate performance and cyclability can be obtained. However, one major problem for these nanoparticles is their relatively low conductivity, especially when they are weakly contacted. To solve this problem, conductive materials such as carbon can be introduced to form shells which will be briefly discussed in the section 2.1. Also, container and conductive matrices which can encapsulate these nanoparticles to form heterogeneous 0-D nanomaterials will be discussed in sections 2.2 and 2.3 respectively.

### 2.1 Core-shell Nanoparticles (Scheme 4a)

Core-shell nanoparticles for lithium ion batteries often refers to a core energy dense nanoparticle coated with a thin carbon shell, which enhances the electrical conductivity, prevents aggregation, improves chemical stability, and buffers the stress of the inner nanoscale active material.<sup>51,70,71</sup>

For example, core-shell nanoparticles with LiFePO<sub>4</sub> core and a carbon shell by *in situ* polymerization has been reported by Wang *et al.*<sup>41</sup> and reviewed by Liu *et al.*<sup>11</sup> These composites

are composed of crystalline LiFePO<sub>4</sub> nanoparticles, 20–40 nm in diameter, covered with 1–2 nm thick carbon shells (Fig. 1b). The specific capacity of this composite was shown to be 169 mAh/g at a 0.6 C discharge rate which is extremely close to the theoretical value of 170 mAh/g for LiFePO<sub>4</sub>. Even at a high, 60 C, discharge rate it delivered a respectable specific capacity of 90 mAh/g (Fig. 1c). The cycle ability of this material was also impressive with the material losing less than 5% of its specific capacity after 1100 cycles at a 0.6 C discharge rate.

Fig. 1a shows the ideal core-shell network of nanoparticles proposed by the author: the LiFePO<sub>4</sub> nanospheres are completely covered by a thin layer of carbon, which serves as the electron pathway and its porous nature allows the lithium ions to diffuse through it.

Kang *et al.* also reported a coated LiFePO<sub>4</sub> nanomaterial with a high rate capability.<sup>29</sup> The particle size of their core LiFePO<sub>4</sub> was about 50 nm in diameter, and an amorphous thin layer was produced on the nanoparticle surface during the heat treatment due to the off-stoichiometry of the starting materials of Li<sub>2</sub>CO<sub>3</sub>, FeC<sub>2</sub>O<sub>4</sub>·2H<sub>2</sub>O, and NH<sub>4</sub>H<sub>2</sub>PO<sub>4</sub>. This material was able to maintain a high specific capacity even at extremely high discharge rates. For example, at a 200 C rate it had a specific capacity greater than 100 mAh g<sup>-1</sup> and at a 400 C rate it had a specific capacity of more than 60 mAh g<sup>-1</sup>. While the nanosizing of the material contributes a little to the high energy retention at high discharge rates, the coating plays a more crucial role. The coating provides an amorphous layer that the Li ions can insert themselves into while waiting to be delivered to the (010) facet of the LiFePO<sub>4</sub> for lithium ion insertion.

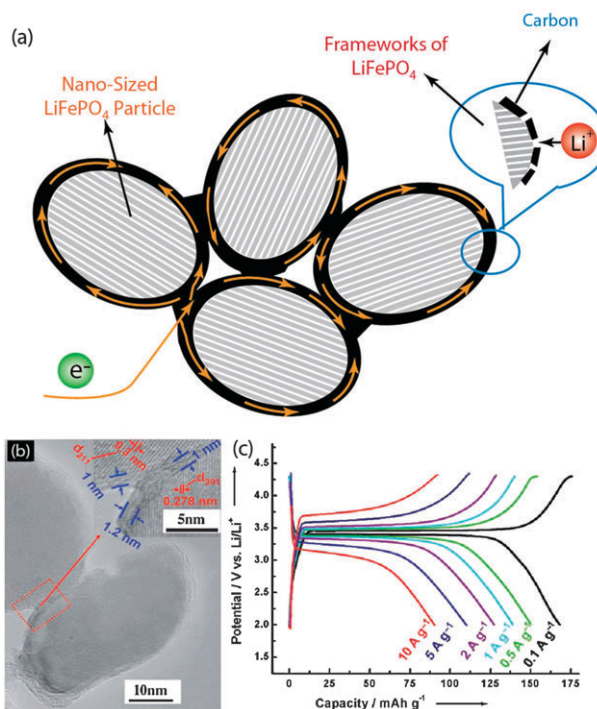


**Fig. 1** (a) Ideal LiFePO<sub>4</sub>/carbon core–shell nanoparticle network and charge transfer mechanism (b) TEM image of the LiFePO<sub>4</sub>/carbon core–shell nanoparticles (c) Charge–discharge tests for the LiFePO<sub>4</sub>/carbon core–shell particles at different current densities in a potential window of 2.0–4.3 V (vs. Li/Li<sup>+</sup>). Adapted and reprinted with permission from ref. 41. Copyright 2008 Wiley-VCH.

Other than carbon, oxides such as MgO, Al<sub>2</sub>O<sub>3</sub> and ZnO have also been coated on cathode materials of lithium ion batteries to prevent direct contact with the electrolyte, which improves their structural stability and suppresses the strain involved during phase transition.<sup>42,43</sup>

## 2.2 Small nanoparticles dispersed and confined in the matrix of larger conductive nanoparticles (Scheme 4c)

Anode materials have recently come into focus that provide a high capacity and hence high energy density. However, these high capacity materials are known to have large volume changes upon lithium ion insertion/removal causing severe crystallite stresses which can reduce the cycle ability of the material.<sup>4,7,10,11</sup> To solve this problem, composite nanoparticles (small high capacity nanoparticles loaded into matrix of much larger conductive nanoparticles) are prepared. The most ideal matrix for this application has been carbon due to its small volume changes and its high electrical and ionic conductivity. This matrix can act as a buffer to relieve the volumetric stresses and can also prevent the agglomeration of the nanoparticles into undesirable microparticles.

An Sb/Al<sub>4</sub>C<sub>3</sub>/C nanocomposite was developed by Park *et al.* using a high-energy mechanical milling technique resulting in an alloying reaction of Al and Sb to form AlSb and then a dealloying reaction of AlSb with carbon to form the more thermodynamically stable Sb and Al<sub>4</sub>C<sub>3</sub> phases.<sup>72</sup> This novel nanocomposite showed a high initial capacity of 687 mAh g<sup>-1</sup> and maintained 76% of this capacity after

200 cycles. A ZnP<sub>2</sub>/C composite nanoparticle with an initial charge capacity of 1340 mAh g<sup>-1</sup> has been reported by the same group.<sup>73</sup>

High surface area  $\alpha$ -Fe<sub>2</sub>O<sub>3</sub>/carbon (HIOC) composite hollow nanoparticles with enhanced lithium storage rates have been synthesized by Chou *et al.*<sup>74</sup> This composite material was able to maintain a specific capacity above 720 mAh g<sup>-1</sup> even after 220 cycles at a high charge/discharge rate of 2 C.

Other than lithium ion batteries, composite nanoparticles are also applied for the supercapacitor electrode materials. For example, microwave-assisted synthesis of poly (3–4-ethyl-enedioxythiophene)/RuO<sub>2</sub>·xH<sub>2</sub>O composite nanoparticles for supercapacitor is reported by Chen *et al.*<sup>75</sup> With only a 1 wt% loading of the RuO<sub>2</sub>, the specific capacitance of the composite was 132.4 F g<sup>-1</sup> compared to only 55.6 F g<sup>-1</sup> for the pristine PEDOT.

## 2.3 Hollow nanosphere loaded with active nanoparticles (Scheme 4b)

Some papers have reported nanoparticles with high Li storage capacity encapsulated into hollow nanospheres. This type of structure provides another way to release the compounded internal stresses of high energy capacity materials. The hollow nanosphere is conductive which keeps the nanoparticles in good electrical contact with each other and the large void volume helps prevent the nanoparticles from agglomerating. More importantly, the large cavity inside this shell can effectively

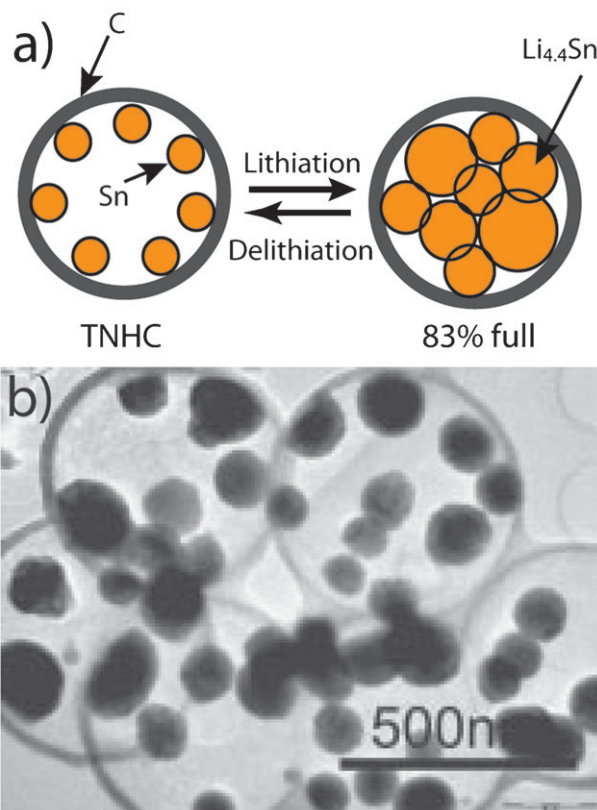


**Fig. 2** (a) Charge/discharge scheme of tin nanoparticles encapsulated with elastic hollow carbon sphere TNHC (b) TEM image of TNHCs. Adapted and reprinted with permission from ref. 76. Copyright 2008 Wiley-VCH.

buffer the volume change brought by the lithium insertion/removal, as shown in Fig. 2a from ref. 63.

Zhang *et al.* reported the synthesis of tin nanoparticles contained within elastic hollow carbon spheres (TNHCs) with a uniform size of about 500 nm.<sup>76</sup> About 5–10 Sn nanoparticles could be found in the hollow carbon spheres. Due to the large empty volume in these 20 nm thick carbon spheres, the Sn nanoparticles could readily expand to fill this space during the lithium insertion (Fig. 2).<sup>76</sup> Consequently, this composite showed decent cycle ability with a high initial capacity of more than 800 mAh g<sup>-1</sup> and after 100 cycles it showed only a moderate decrease in its specific capacity to 550 mAh g<sup>-1</sup>. Single tin nanoparticles loaded into hollow carbon nano-containers has also been reported by Lee *et al.*<sup>77</sup>

SnO<sub>2</sub> nanoparticles inside crystalline carbon hollow nanospheres have been synthesized using a microwave-assisted hydrolysis technique by Wang *et al.*<sup>78</sup> This composite material consisted of 25.6 wt% SnO<sub>2</sub>. The initial specific capacity was found to be 468 mAh g<sup>-1</sup> with only a 8.6% drop in this capacity after 60 cycles, showing good capacity retention which is an improvement over previous similar works.<sup>77</sup>

Lou *et al.* have reported a double-shelled hollow sphere.<sup>79</sup> Instead of loading SnO<sub>2</sub> nanoparticles into the hollow carbon nanosphere, a mesoporous SnO<sub>2</sub> layer is sandwiched between two carbon layers. This material showed a higher capacity than pristine hollow SnO<sub>2</sub> spheres and also a higher capacity than the theoretical capacity of the commercially applied graphite anodes even after 50 cycles.

### 3. One-dimensional (1-D) heterogeneous nanostructures

Compared to the 0-D nanostructures, 1D nanostructures provide a direct pathway for efficient charge transport along its micro-scale axis, while the two radically small nano-scale dimensions have similar advantages of 0D nanoparticles, *i.e.* fast rate capabilities. Owing to the above unique merits, 1D nanostructures have been intensively studied for applications in electrochemical energy storage devices.<sup>22,27,32,34,46,47,53–57,61–66</sup> However, as we mentioned earlier, 1-D or one-dimensional nanomaterials with a single component are facing similar problems experienced by all single component nanosystems such as low conductivities, weak mechanical stabilities, undesired surface properties, weak cyclabilities, *etc.* Therefore, heterogeneous 1-D nanostructures with various forms have been proposed to circumvent the above limitations. Here we will discuss them in detail. We have separated them into two major categories: disordered networks composed of 1-D heterogeneous nanostructures (section 3.1), and ordered arrays of 1-D heterogeneous nanostructures (section 3.2). We will tend to break each major category into a few sub categories based on the sub-level nanostructure such as coaxial nanowires, double-shell nanotubes, composite nanowires/nanotubes, *etc.*

#### 3.1 Disordered network of 1-D heterogeneous nanostructures

Most existing synthetic methods can only produce 1-D nanomaterials in a random order: thus obtained nanowires/nanotube are irregularly oriented and connected to form a disordered network. By introducing multiple precursors when

synthesizing these nanomaterials or subsequently modify them by surface treatment, various forms of disordered 1-D heterogeneous nanostructures can be acquired.

**3.1.1 Disordered carbon nanotubes (CNT) and carbon nanofibers (CNF) modified with active electrode materials (Scheme 4d).** When electrode materials are coated on the CNTs, the charge transport can be facilitated by the highly conductive CNTs, and the nanoscale thickness coating on the CNTs will allow fast rate capabilities, thus carbon nanotubes are widely used as the current collecting material.<sup>45,80–87</sup> This strategy is similar to the carbon coated core–shell nanoparticles, though in that case, carbon is coated on the surface of the active material instead of serving as the conductive core.

Zhang *et al.* have reported the conformal loading of SnO<sub>2</sub> nanoparticles onto a net-like matrix of CNTs.<sup>45</sup> Due to this uniform coating of SnO<sub>2</sub> (Fig. 3), good electrical contact between the SnO<sub>2</sub> and the CNT matrix is maintained during cycling allowing for the volume changes associated with lithium-ion intercalation/deintercalation. These nanocomposites showed an initial charge capacity of 851 mAh g<sup>-1</sup> which increased upon cycling to a capacity of more than 950 mAh g<sup>-1</sup> after 50 cycles. This capacity increase was attributed to a high charge cut-off potential of 3 V which may cause an undesirable reaction of Sn with the SEI layer.

An *et al.* have fabricated a single wall carbon nanotube-polypyrrole (SWNT-Ppy) nanocomposite which was shown to be capable of improving the specific capacitance of supercapacitors.<sup>84</sup> Ppy was uniformly coated on these high

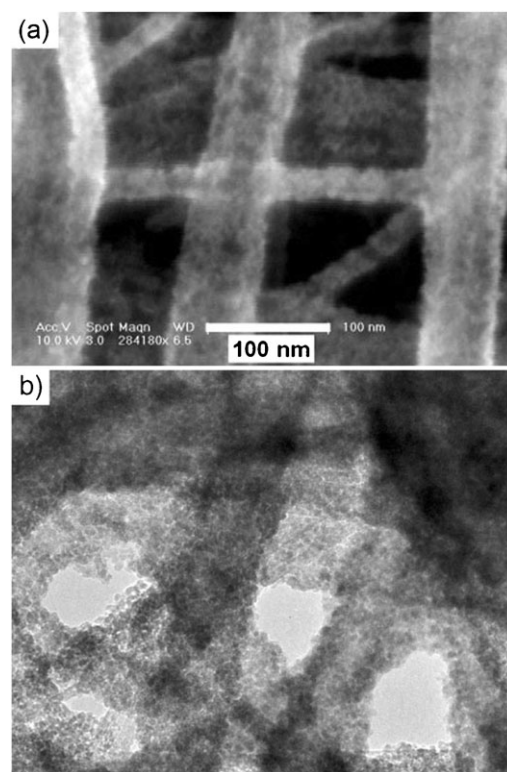


Fig. 3 (a) SEM (b) TEM images of SnO<sub>2</sub>–CNT composite sheet. Adapted and reprinted with permission from ref. 45. Copyright 2009 Wiley-VCH.

surface area SWNTs resulting in an increase in supercapacitive active sites along the Ppy chains. A maximum specific capacitance of 265 F/g was shown for the SWNT-Ppy nanocomposite that contained 15 wt% SWNTs.

Cui *et al.* prepared carbon–silicon core–shell nanowires by using a CVD method to coat amorphous silicon onto a carbon nanofibers network.<sup>86</sup> These heterogeneous nanowires showed a high initial storage capacity of greater than 2000 mAh/g and good 80% capacity retention after 30 cycles.

**3.1.2 Disordered coaxial nanowires (Non CNT network based).** Besides carbon nanotubes, other materials have also been successfully applied as the conductive network to support the electroactive materials.<sup>50,88–90</sup>

For example, Zhou *et al.* reported a heterostructured Si/TiSi<sub>2</sub> composite, which is formed by attaching Si nanoparticles to a highly conductive TiSi<sub>2</sub> matrix (Fig. 4a and b).<sup>90</sup> The TiSi<sub>2</sub> matrix consisting of a network of TiSi<sub>2</sub> nanowires provides the structural support and can speed electron transfer due to its high conductivity. The similarities between the crystal structures of TiSi<sub>2</sub> and Si make the interfacing of Si with TiSi<sub>2</sub> relatively simple. Fast charge/discharge rates without significant capacity fading were achieved with this composite. In fact, at the high charge rate of 8400 mA/g, a high capacity of about 1000 mAh/g was obtained with 99% capacity retention after 100 cycles (Fig. 4c).

Cui *et al.* have synthesized silicon nanowires with crystalline cores and amorphous shells directly on a conductive substrate

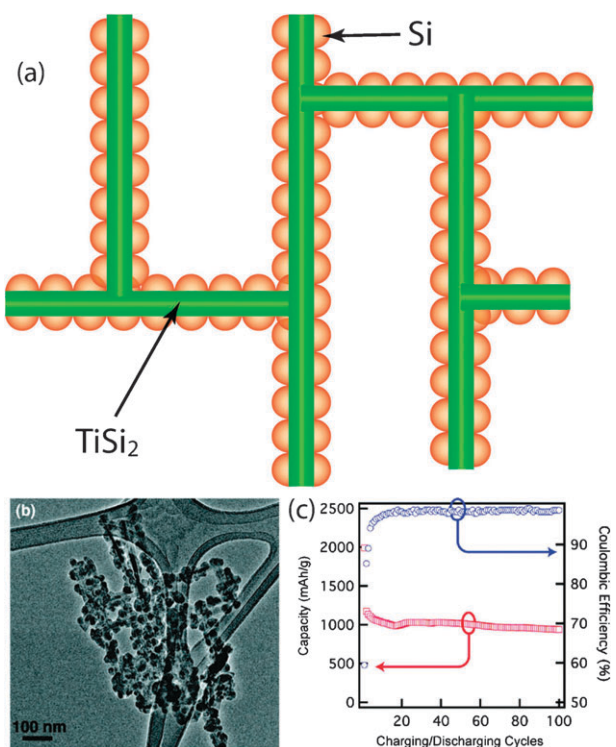


**Fig. 4** (a) Schematic of the Si/TiSi<sub>2</sub> heterogeneous nanostructure. (b) TEM picture manifests the particulate nature of the Si coating on TiSi<sub>2</sub> NNs. (c) Charge capacity and Coulombic efficiency of the Si/TiSi<sub>2</sub> heteronanostructure with an 8400 mA/g charge/discharge rate tested between 0.150 and 3.00 V. Adapted and reprinted with permission from ref. 90. Copyright 2010 American Chemical Society.

using a simple CVD process.<sup>88</sup> Due to the difference of lithiation potentials, the amorphous Si shells can be selectively lithiated with the crystalline Si cores only being used for their conductivity and mechanical support. A high initial charge capacity of greater than 1000 mAh/g was exhibited for these core–shell nanowires with only about a 10% capacity fade after 1000 charge/discharge cycles.

Yan *et al.* were able to coat SnO<sub>2</sub> nanowires with amorphous MnO<sub>2</sub> by simple immersion of the SnO<sub>2</sub> nanowires into a hot KMnO<sub>4</sub> bath.<sup>89</sup> A maximum specific capacitance of 637 F g<sup>-1</sup> was calculated for the MnO<sub>2</sub> coating at a scan rate of 2 mV s<sup>-1</sup> in an aqueous Na<sub>2</sub>SO<sub>4</sub> solution. This material showed high power capabilities, with a high energy density of 35.4 Wh kg<sup>-1</sup> being obtained at the high power density of 25 kW kg<sup>-1</sup>. The SnO<sub>2</sub>/MnO<sub>2</sub> heterogeneous electrode showed excellent cyclic ability retaining 98.8% of its capacitance after 2000 cycles.

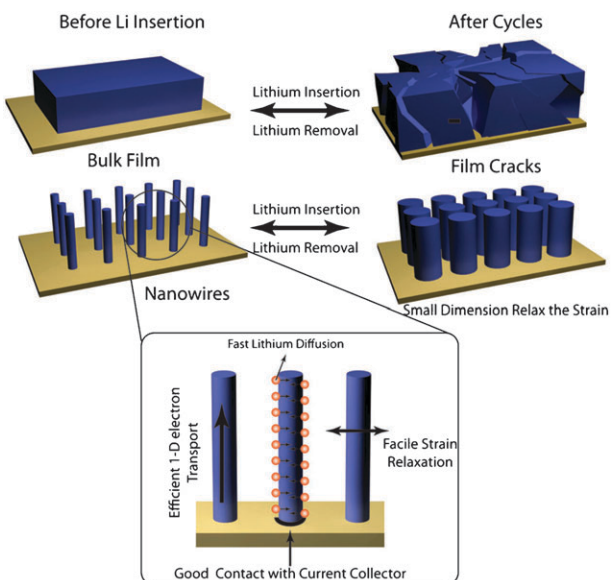
**3.1.3 Disordered composite nanowires.** This type of material consists of nanowires or nanofibers that contain two or more randomly ordered materials. These materials are more homogeneously mixed compared to the coaxial nanowires. To date, there are only a few existing reports showing this type of nanostructure for applications in electrochemical energy storage devices.<sup>91–93</sup>

Ji *et al.* prepared carbon/silicon (C/Si) composite nanofibers by first electrospinning polyaniline nanofibers containing silicon nanoparticles and then thermally treating these fibers to decompose the polyaniline to carbon.<sup>91</sup> The C/Si composite nanofibers were then tested as anode materials for lithium ion batteries. If the Si wt% was kept below 15%, this composite could achieve large reversible capacities of about 1800 mAh g<sup>-1</sup> with good cycling performance; however, at larger Si wt% the individual Si nanoparticles can agglomerate causing significant capacity loss and lower cyclic abilities.

A 1-D nanostructured manganese dioxide/polypyrrole (MnO<sub>2</sub>/PPy) composite was prepared by Li *et al.* by addition of MnO<sub>2</sub> nanoparticles during the chemical oxidation polymerization of pyrrole.<sup>92</sup> The obtained composite maintained a specific capacitance of 320 F/g after 500 charge–discharge cycles in the potential range of -0.4 to 0.6 V in a neutral pH KCl electrolyte.

### 3.2 Well ordered arrays of 1-D nanostructured materials

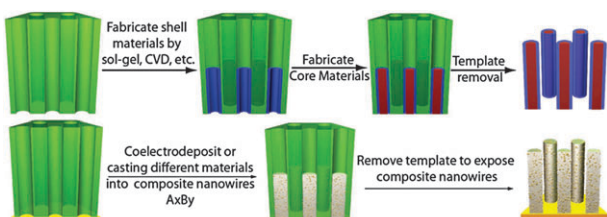
Ordered arrays of 1-D nanostructured materials can be synthesized on a substrate or in a nanoscale pore-sized template by the “bottom-up” growth approach, *i.e.* the growth direction of the 1-D nanostructure is well controlled, in most cases, perpendicular to the substrate such as a current collector. Since each nanowire is directly contacted with the current collector, there is an efficient transfer of electrons to each and every 1-D nanostructure in the nanowire array.<sup>22,32,34,46,55,60,61,63,65,66</sup> Due to this electronic efficiency, there is no need for extra binders or conductive additives which are used for most other electrode materials. The void volume between the neighboring 1-D nanomaterials can allow for easy penetration of the electrolyte resulting in a high ion flux and can also accommodate a materials volume change during lithium insertion/removal resulting in better cycle ability (Scheme 5). Such volume change can be even better



**Scheme 5** Advantages of using arrays of 1-D nanomaterials *versus* their bulk counterparts as electrode materials for electrochemical energy storage.

alleviated if hollow nanotubes are utilized. By combining different materials into ordered 1-D nanostructures, arrays of 1-D heterogeneous nanostructures can be formed, which have been shown to exhibit synergic properties (*e.g.* high conductivity) or functionalities (better mechanical stabilities). Due to the above advantages, ordered arrays of 1-D heterogeneous nanostructures are currently considered as one of the most promising candidates for future electrode materials for electrochemical energy storage devices.<sup>32,34,46,63,65,66</sup>

Template synthesis using anodized aluminium oxide, AAO, as the mold is one of the most ideal methods for synthesizing arrays of 1-D heterogeneous nanostructures. AAO is chosen because of its facile synthesis, controllable pore-size, well-ordered pores, and the high density of its pores along with its amenable ability to be removed with either acidic or basic solutions.<sup>54,58,59,94</sup> In short, one side of the alumina template can be first coated with a desired conductive material, which will serve as the current collector later on, then different materials can be simultaneously or subsequently loaded into the perfect aligned nanochannels to form well ordered arrays of heterogeneous 1-D nanostructures (Scheme 6). Martin's group is the pioneering group who developed this template synthesis method and showed the excellency of 1-D single phase and heterogeneous nanostructures for electrochemical energy storage materials.<sup>27,54,63,66,95–99</sup>



**Scheme 6** Template synthesis of arrays of 1-D heterogeneous nanostructures with different composite morphologies.

Other than template synthesis, a well controlled CVD method is another popular method to synthesize well ordered 1-D nanomaterials. This method can be used to create materials such as carbon nanotubes, which can be further loaded with silicon nanoparticles and manganese oxide nanoflowers to form 1-D heterogeneous nanostructures.<sup>47,100</sup>

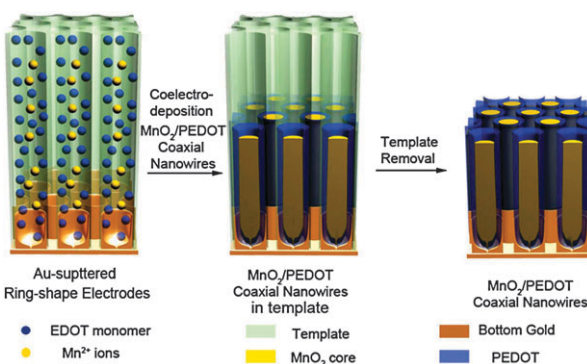
The following subsections will list a few types of ordered arrays based on 1-D heterogeneous nanomaterials according to their sub-level nanostructure.

**3.2.1 Ordered arrays of coaxial nanowires.** Our group has recently reported  $\text{MnO}_2/\text{poly}(3,4\text{-ethylenedioxythiophene})$  (PEDOT) coaxial nanowires synthesized by a one-step electrochemical deposition process using a porous alumina template.<sup>46</sup> The studies of the growth mechanism for this coaxial nanowire revealed that the shapes of the nano-electrodes at the bottom of the alumina template play a very important role in the formation of the  $\text{MnO}_2$  core and PEDOT shell: PEDOT tends to grow on the ring-shaped electrode due to the sharp edges while  $\text{MnO}_2$  is more likely to deposit on the smooth surfaces of the flat top electrodes.

The phase segregation of  $\text{MnO}_2$  and PEDOT leads to simultaneous growth of  $\text{MnO}_2$  core and PEDOT shell resulting in coaxial nanowires. (Scheme 7) Fig. 5a–d shows the SEM, TEM images and EDS mapping of the  $\text{MnO}_2/\text{PEDOT}$  coaxial nanowires.

In this composite, the  $\text{MnO}_2$  core is utilized for its high energy density, while the PEDOT shell is applied for its high conductivity and its porous and flexible nature. The PEDOT shell facilitates electron transport and ion diffusion into the energy dense  $\text{MnO}_2$  core and protects the core from structural collapse and breaking. These combined properties result in a synergic composite that has very high specific capacitances at high current densities as opposed to pure  $\text{MnO}_2$  nanowires, PEDOT nanowires, and a  $\text{MnO}_2$  thin film (Fig. 6).

When one controls the applied potential during the electro-deposition, a change in the nanostructure's composition as well as its electrochemical properties happens. This change allows for a tuning of the nanowire's composition to try to produce the best electrochemical properties possible. For example, coaxial nanowires with various PEDOT shell thicknesses (25 to 100 nm) can be obtained by adjusting this applied potential, as shown in Fig. 5e.



**Scheme 7** Growth mechanism of the coaxial  $\text{MnO}_2/\text{PEDOT}$  nanowire. Adapted and reprinted with permission from ref. 46. Copyright 2008 American Chemical Society

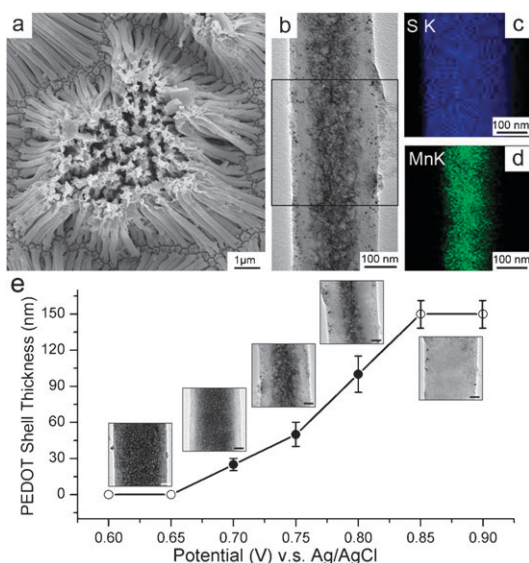


**Fig. 5** (a) SEM image of  $\text{MnO}_2/\text{PEDOT}$  coaxial nanowires (synthesized at 0.75 V). (b) TEM image from a single coaxial nanowire (synthesized at 0.75 V). (c and d) EDS maps of S and Mn from the boxed area in Fig. 5b. (e) PEDOT shell thickness variation with applied potential. Scale bar, 50 nm. Adapted and reprinted with permission from ref. 46. Copyright 2008 American Chemical Society.

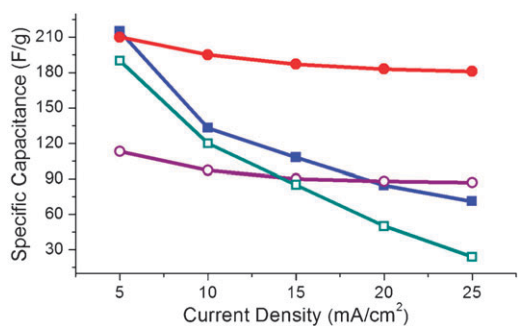


**Fig. 6** Specific capacitance of  $\text{MnO}_2$  nanowires (closed blue square), PEDOT nanowires (open purple dots),  $\text{MnO}_2$  thin film (open green square), and  $\text{MnO}_2/\text{PEDOT}$  coaxial nanowires (closed red dots) at different charge/discharge current densities. Adapted and reprinted with permission from ref. 46. Copyright 2008 American Chemical Society.

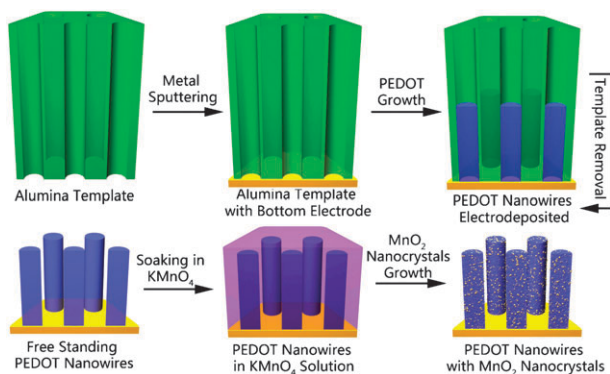
**3.2.2 Arrays of composite nanowires/nanotubes.** Composite nanotubes composed of  $\text{LiMn}_2\text{O}_4$  with polypyrrole has been fabricated by the Martin group.<sup>63</sup> First, spinel  $\text{LiMn}_2\text{O}_4$  nanotubes of 200 nm outer diameter were prepared by thermal decomposition of an aqueous solution containing lithium nitrate and manganese nitrate at 1:2 molar ratio using a nanoporous alumina membrane as a template. Then, after the template is removed, polypyrrole was coated on these  $\text{LiMn}_2\text{O}_4$  nanotube to form a composite nanotube array. The polypyrrole-coated  $\text{LiMn}_2\text{O}_4$  tubule electrodes exhibited higher capacities than the polypyrrole-coated  $\text{LiMn}_2\text{O}_4$  thin-film electrode prepared under the same conditions, especially under high charge/discharge current density. Such high capacity can be attributed to the high specific surface area of the nanotube electrode and a decrease in the thickness of

$\text{LiMn}_2\text{O}_4$  solid phase resulting in a short diffusion length for the  $\text{Li}^+$  ions during the charging and discharging reactions. The same group has also reported  $\text{LiFePO}_4/\text{carbon}$  composite nanowires as a high-rate cathode.<sup>66</sup>

Our group has recently reported the loading of finely dispersed  $\text{MnO}_2$  nanoparticles into PEDOT nanowires by simply soaking PEDOT nanowires into a potassium permanganate solution (Scheme 8, Fig. 7).<sup>44</sup>

As a supercapacitor material, the  $\text{MnO}_2$  nanoparticles in these  $\text{MnO}_2$  nanoparticle-enriched PEDOT nanowires show a very high specific capacitance (410 F/g) due to their extremely high exposed surface area resulting from their small size.

Fig. 8b demonstrates that these composite nanowires can also serve as potential cathode materials for lithium ion batteries. It is shown that the charge capacity of the PEDOT nanotube matrix was increased over 4 times after the loading of the  $\text{MnO}_2$  nanoparticles. The charge storage capacity that



**Scheme 8** Synthesis of  $\text{MnO}_2$ -NP/PEDOT composite nanowires. Adapted and reprinted with permission from ref. 44. Copyright 2010 American Chemical Society.

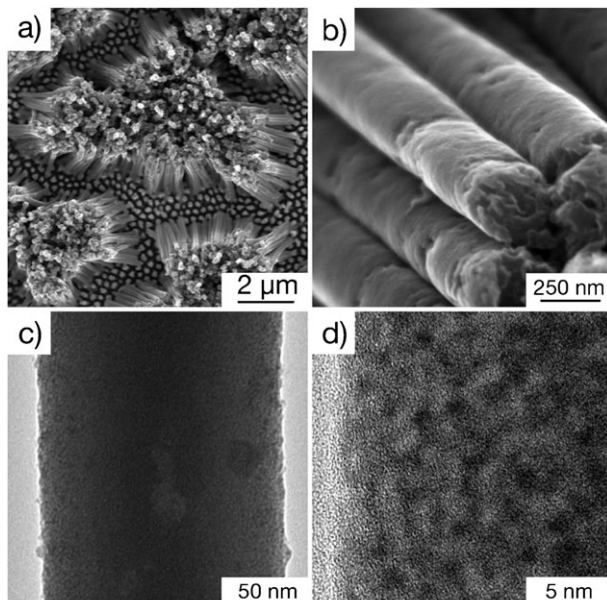


**Fig. 7** (a,b) SEM and (c,d) TEM images at different magnifications of PEDOT nanowires after being treated with  $\text{KMnO}_4$  (10 mM) for 10 min. Adapted and reprinted with permission from ref. 44. Copyright 2010 American Chemical Society.

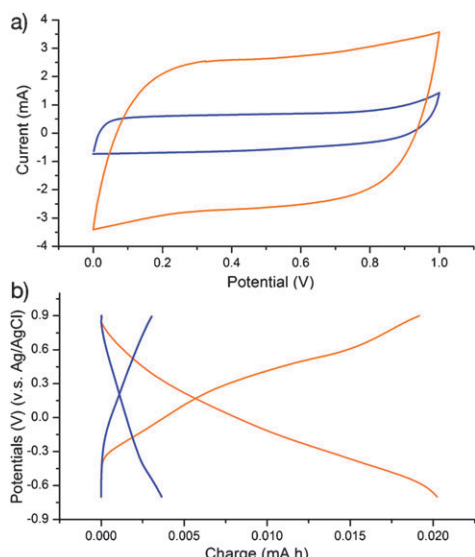
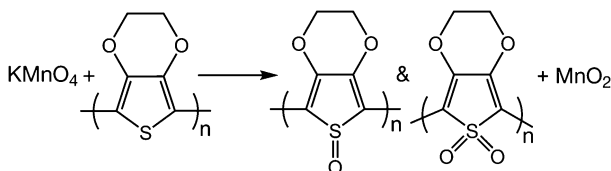


**Fig. 8** (a) Cyclic voltammograms of PEDOT nanowires before (blue) and after (orange) 10 mM KMnO<sub>4</sub> treatment (10 min) (b) Galvanostatic charge/discharge curves of PEDOT nanowires (blue) and MnO<sub>2</sub>-NP/PEDOT nanowires (orange) at current density of 1.25 mA/cm<sup>2</sup>. Adapted and reprinted with permission from ref. 44. Copyright 2010 American Chemical Society.

can be attributed to the MnO<sub>2</sub> nanoparticles can be calculated as 300 mAh g<sup>-1</sup>, which is very close to the theoretical capacity of MnO<sub>2</sub> (308 mAh/g). This corresponds to a lithium insertion coefficient of 0.97 or Li<sub>0.97</sub>MnO<sub>2</sub>. This high capacity at the high charge/discharge rate of 10 C can be attributed to the short diffusion path lengths and high flux of lithium ions associated with the small size of these nanoparticles.

A major advantage of this synthetic method is the ease of synthesis of these MnO<sub>2</sub> nanoparticles. There is no need for any complicated steps but just a simple chemical redox process. When the PEDOT nanowires enter the solution, the oxidant, KMnO<sub>4</sub>, is reduced to MnO<sub>2</sub> by oxidizing the sulfur functional group of PEDOT (Scheme 9). This provides a seed layer for the natural formation and growth of MnO<sub>2</sub> nanoparticles into the nanoscale pores of the nanowires.

Compared to the MnO<sub>2</sub>/PEDOT coaxial nanowires mentioned in Section 3.2.2, the MnO<sub>2</sub> and PEDOT materials are more uniformly mixed in these heterogeneous nanowires. These infused MnO<sub>2</sub> nanoparticles have an ultrahigh surface area as mentioned earlier, which enables an enhancement of the energy storage capacity of the PEDOT nanowires of up to 4 times (Fig. 8a) (e.g. to a high specific capacitance of 252 F/g), causing only minimal volume expansion in the polymer. The highly conductive and porous PEDOT matrix facilitates fast



**Scheme 9** Reduction of KMnO<sub>4</sub> by PEDOT to form MnO<sub>2</sub>. Adapted and reprinted with permission from ref. 44. Copyright 2010 American Chemical Society.

electronic and ionic migration to the MnO<sub>2</sub> nanocrystals and prevents them from agglomerating. These combined properties result in synergic MnO<sub>2</sub> nanoparticle-enriched PEDOT nanowire that has a high specific capacitance even at a high charge/discharge rate.

PEDOT/RuO<sub>2</sub> nanotube composites are another example of heterogeneous 1-D nanomaterial arrays reported by our group.<sup>32</sup> RuO<sub>2</sub> was chosen here to be combined with PEDOT due to its well researched supercapacitor applications which have shown ultra-high pseudocapacitances.<sup>101</sup> Arrays of these nanotube composites were synthesized by a step-wise method. First, PEDOT nanotubes were grown in an alumina template by electropolymerization. RuO<sub>2</sub> was then electrodeposited into this porous PEDOT nanotube matrix resulting in the formation of composite RuO<sub>2</sub>/PEDOT nanotubes. The charge/discharge mechanism of these composite nanotubes is illustrated in Fig. 9a.

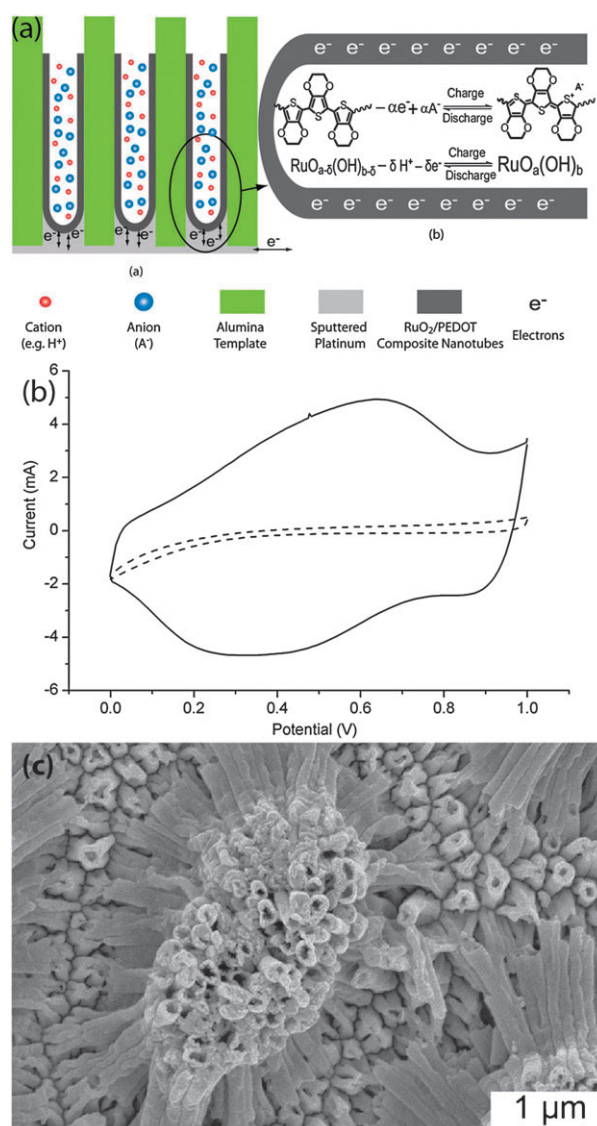


**Fig. 9** (a) Charge-storage mechanism of RuO<sub>2</sub>/PEDOT composite nanotubes. (b) Cyclic voltammograms of PEDOT nanotubes (—) and RuO<sub>2</sub>/PEDOT composite nanotubes (—) (c) SEM images of the RuO<sub>2</sub>/PEDOT nanotubes. Adapted and reprinted with permission from ref. 32. Copyright 2010 the Owners Societies.

Doping the PEDOT nanotube matrix with RuO<sub>2</sub> improved the specific capacitance of the PEDOT to 640 F g<sup>-1</sup> (Fig. 9b) even at a high power demand of 20 kW kg<sup>-1</sup>. This high power capability results from the high surface area and short diffusion path lengths of the nanotubular structure, while the large increase in capacitance results from the efficient utilization of RuO<sub>2</sub> resulting in a specific capacitance attributable to the RuO<sub>2</sub> of 1217 F g<sup>-1</sup>. The PEDOT nanotube and the later deposited RuO<sub>2</sub> were found to mechanically enhance each other. Whereas, the PEDOT nanotubes provide a flexible substrate for the RuO<sub>2</sub> loading which can prevent the RuO<sub>2</sub> nanostructures from breaking and detaching from the current collector when the alumina template is removed and the more rigid RuO<sub>2</sub> helps the PEDOT nanotubes maintain their nanotubular shapes by providing the stability to keep their ends from agglomerating which would eliminate the benefits of this nanotubular structure (Fig. 9c).

**3.2.2 Current collector based order arrays of 1-D nanomaterials.** When the current collector are transformed into 1-D nanowire or nanotube arrays, the electrode materials can be subsequently coated on these nanowires or loaded into these nanotubes to form coaxial nanowires or tube-in-tube composite electrodes. For example, Taberna *et al.* has prepared a Fe<sub>3</sub>O<sub>4</sub> and Cu composite electrode for lithium ion battery applications by using a two-step electrochemical synthesis process.<sup>34</sup> First, an array of 200 nm diameter copper nanorods acting as the current collector was grown by electrodeposition using an anodized aluminium template. After the template was removed, Fe<sub>3</sub>O<sub>4</sub> was deposited onto the surface of each Cu nanorod by applying a reducing current ( $-5 \text{ mA cm}^{-2}$ ) in an Fe<sup>3+</sup> solution (Fig. 10a and b). At a high 8C charge/discharge rate, the composite was still able to retain 80% of its initial capacity. The capacity of the electrode was shown to increase as the loading of the magnetite increased (Fig. 10c) Due to its mechanical stability, this composite was able to retain its full capacity after many cycles even at a high rate. The same group has also reported an electrode based on Ni<sub>3</sub>Sn<sub>4</sub> nanoparticles deposited on Cu nanorod arrays that display excellent cyclability and rate capability.<sup>102</sup>

Template synthesized carbon nanotubes,<sup>103</sup> nickel nanowires<sup>28</sup> have also been applied as ordered 1-D current collector arrays.<sup>104</sup> For example, Reddy *et al.* reported coaxial manganese oxide/carbon nanotube (CNT) arrays synthesized using a porous alumina template and their application as a lithium battery material.<sup>65</sup> The composite arrays showed an initial charge capacity of 2170 mAh/g that began to stabilize at about 500 mAh/g after 15 cycles. This high capacity can be attributed to both the insertion/extraction of lithium ions for the CNTs and the formation/decomposition reaction of Li<sub>2</sub>O for the MnO<sub>2</sub> nanotubes.

Hu *et al.* prepared a nanoarchitected electrode composed of V<sub>2</sub>O<sub>5</sub>/carbon tube-in-tube (CTIT) nanostructures<sup>105</sup> which has been reviewed by Liu *et al.*<sup>11</sup> The CTIT is used here as a conductive substrate for the energy dense V<sub>2</sub>O<sub>5</sub> material and also allows easy penetration of the electrolyte around the V<sub>2</sub>O<sub>5</sub> (Fig. 11b). An initial capacity of 280 mAh g<sup>-1</sup> was obtained at a C/2.5 charge/discharge rate with only a 5% capacity fade after 20 cycles.

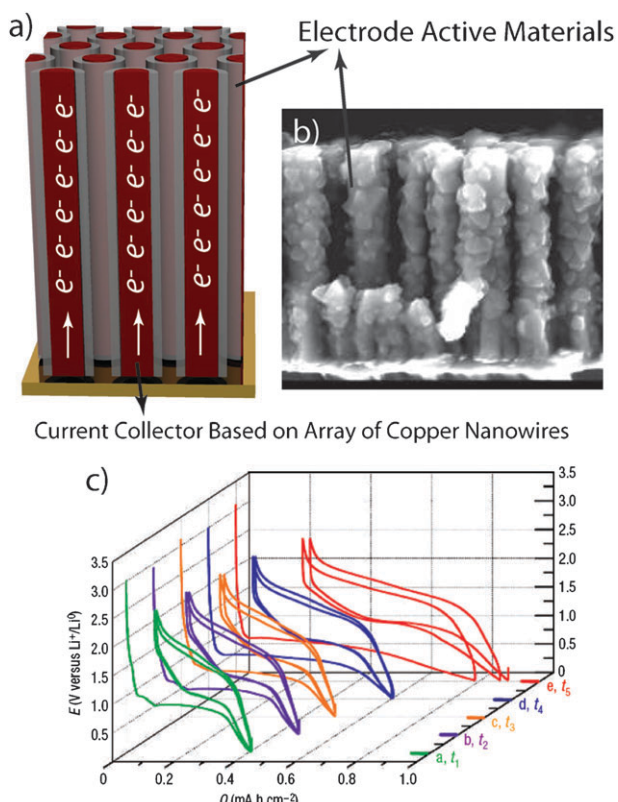


**Fig. 10** (a) Schematic view of current collector based on array of copper nanowires. (b) SEM cross-sectional views of current collector after Fe<sub>3</sub>O<sub>4</sub> deposits. (c) Potential-capacity profiles for the as-prepared copper-supported Fe<sub>3</sub>O<sub>4</sub> deposits galvanostatically cycled at a rate of 1 Li<sup>+</sup> 2 h versus Li with  $t_1 - t_5$  ( $t_1 = 120 \text{ s}$ ,  $t_2 = 150 \text{ s}$ ,  $t_3 = 180 \text{ s}$ ,  $t_4 = 230 \text{ s}$  and  $t_5 = 300 \text{ s}$ ) corresponding to the Fe<sub>3</sub>O<sub>4</sub> material electrodeposition time. Adapted and reprinted with permission from ref. 34. Copyright 2006 Nature Publishing Group.

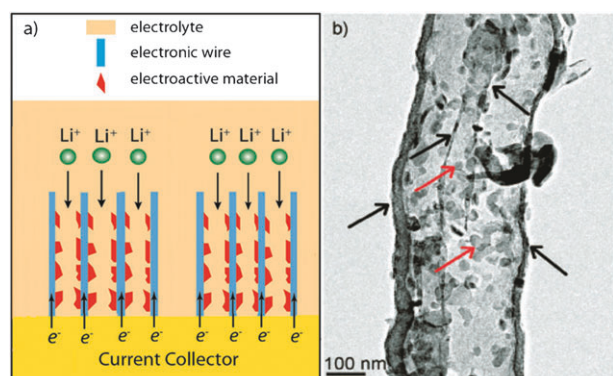
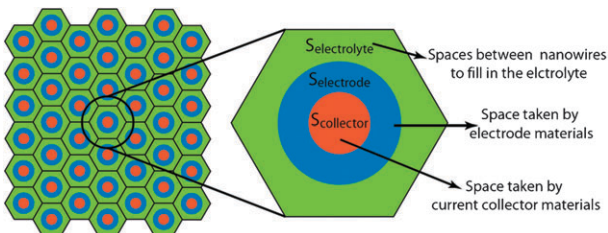


**Fig. 11** (a) Schematic representation of the desired design based on an efficiently mixed-conducting network. (b) Typical TEM image of the V<sub>2</sub>O<sub>5</sub>/CTIT nanocomposites showing that most of the V<sub>2</sub>O<sub>5</sub> nanoparticles are encapsulated within CTIT. Adapted and reprinted with permission from ref. 105. Copyright 2009 Wiley-VCH.

Cao's group has prepared Ni–V<sub>2</sub>O<sub>5</sub>·nH<sub>2</sub>O core–shell nanowire arrays for lithium–ion battery applications.<sup>106</sup> These Ni–V<sub>2</sub>O<sub>5</sub>·nH<sub>2</sub>O composite nanorods were prepared by first template synthesizing Ni nanorods and then electrophoretically depositing a 30–50 nm layer of V<sub>2</sub>O<sub>5</sub>·nH<sub>2</sub>O onto each



**Scheme 10** Imagined unit cells of an alumina template each loaded with heterogeneous nanowire with the electrolyte filling the volume left after template removal.

Ni nanorod's surface. This thin  $V_2O_5 \cdot nH_2O$  layer was shown to intercalate an incredibly high lithium insertion coefficient of 3.1 ( $Li_{3.1}V_2O_5 \cdot nH_2O$ ) which can be attributed to the short diffusion path lengths and high surface area of the material. Both the power and energy density of this material was observed to be over one order of magnitude greater than that of a planar  $V_2O_5$  material.

It is worth noting that when these arrays of 1-D current collectors are fabricated by template synthesis, an optimization is necessary for the following: the spaces between the nanowires, the diameter of the current electrode and the volume of the electrode material. Scheme 10 illustrates imagined individual unit cells of an alumina template, with each containing a single heterogeneous coaxial nanowire (current collector core and active materials shell) with the electrolyte filling in the volume left after dissolution of the template.

First, the diameter or area of the current collector core ( $S_{\text{collector}}$ ) needs to be optimized. If the  $S_{\text{collector}}$  is too small it will result in a high electrical resistance. If the  $S_{\text{collector}}$  is too big it will occupy too much of the valuable volume. For example, a commercially available membrane from Whatman (200 nm pore size) has a porosity of 60%, which suggests that it is not suitable for fabricating solid nanowire current collectors, because too much of the volume and weight will be occupied by the current collector. Therefore, an alumina template with less porosity, which can be synthesized in one's own lab, may be required, or the current collecting materials may be fabricated in the forms of nanotubes. These nanotubes will not occupy as much of the needed space when compared to the solid nanowires. Second, the ratio of the space taken by the electrode material ( $S_{\text{electrode}}$ ) to the space taken by the electrolyte ( $S_{\text{electrolyte}}$ ) needs to be carefully considered. Electrode materials require enough loading as to maximize the volumetric energy density of the electrode while not taking over the space needed for the electrolyte, which could cause depletion of lithium ions in the nano-sized channel.

As mentioned earlier, in addition to template synthesis, other synthetic methods such as well controlled CVD have also been applied to fabricate well ordered arrays of 1-D nanomaterials, such as carbon nanotubes,<sup>100,107,108</sup> which have the potential to be used as the current collector.

For example, Zhang *et al.* have prepared a vertically aligned carbon nanotube array (CNTA) framework and modified them with well-dispersed manganese oxide nanoflowers by electrodeposition (Fig. 12a and b).<sup>47</sup> As a supercapacitor material, these manganese oxide/CNTA composite electrodes exhibited high power capabilities with a 50.8% capacity

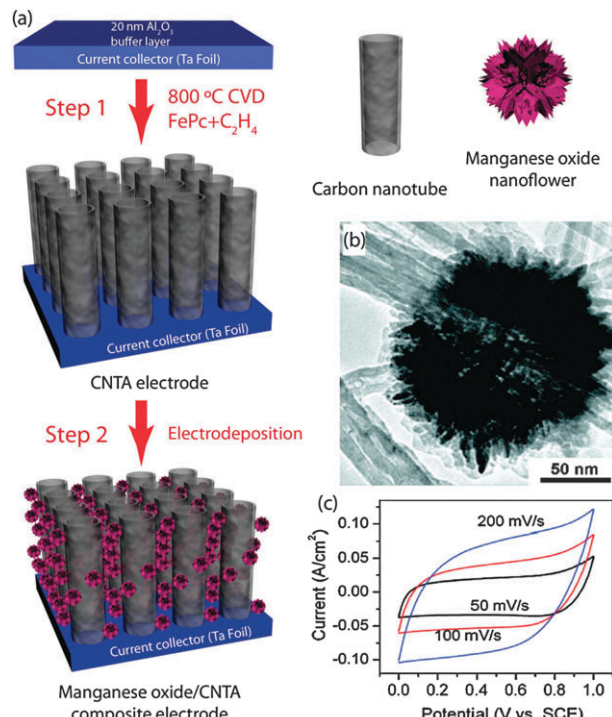


**Fig. 12** (a) Procedure for the preparation of manganese oxide/CNTA composite electrode. (b) TEM image of a manganese oxide nanoflower. (c) CV curves of the manganese oxide/CNTA composite electrode. Adapted and reprinted with permission from ref. 47. Copyright 2008 American Chemical Society.

retention when the current density was increased from 10  $A/g$  to 77  $A/g$ . After 20 000 cycles, the composite material showed an impressive 97% capacity retention. The cyclic voltammetry curves showed the material's supercapacitive nature even at high scan rates (Fig. 12c). These impressive electrochemical properties can be attributed to the CNTA's electronic conductivity, well-ordered pores, and mechanical sturdiness.

Wang *et al.* reported the synthesis of multiwalled CNT arrays containing crystalline Si nanoparticles by a two-step CVD method. This composite array exhibited an initial discharge capacity of 2553  $mAh/g$  which was sustained above 2000  $mAh/g$  after 25 cycles. Even at a high discharge rate of 2.5 C, the compositing displayed capacities above 1000  $mAh/g$ .<sup>100</sup>

Doping is another way to improve the intrinsic properties of single-phase 1-D nanostructures. For example, Ghicov *et al.* was able to dope titania nanotubes with Niobium atoms to produce an ion intercalation host structure with increased lattice spacing,<sup>109</sup> after it was shown that 1D  $TiO_2$  nanostructures could be used as lithium intercalation materials.<sup>53,110,111</sup> The authors were able to show that the kinetics of Li-ion insertion was enhanced by the reduction of the diffusion/migration barrier resulting from this increase in lattice spacing.

#### 4. Two-dimensional (2-D) heterogeneous nanostructures

Two-dimensional (2-D) nanomaterials, often referred to as nanosheets or nanofilms, haven't received much attention

throughout the research of electrochemical energy storage<sup>112–114</sup> until the recent reports of applying graphene<sup>115,116</sup> and its composites<sup>117–122</sup> as electrode materials for lithium ion battery.

Graphene, a newly discovered 2-D nanofilm, is composed of a one-atom-thick planar sheet of  $sp^2$ -bonded carbon atoms that are densely packed into a honeycomb crystal lattice. This material exhibits better electrical conductivities than graphitic carbon, has a high surface area of over  $2600\text{ m}^2/\text{g}$ , an elevated chemical tolerance, and a broad electrochemical window that is favorable for applications in electrochemical energy storage devices. For example, a large reversible Li ion storage ( $540\text{ mAh/g}$ ) for a graphene nanosheet is reported by Yoo *et al.*<sup>115</sup> Ruoff *et al.* reported that supercapacitors based on multilayered graphene display a specific capacitance of  $135\text{ F g}^{-1}$  in an aqueous electrolyte solution.<sup>116</sup>

Paek *et al.* assembled graphene/SnO<sub>2</sub> composite electrodes by reassembling graphene nanosheets in the presence of SnO<sub>2</sub> nanocrystals (Fig. 13a).<sup>117</sup> SEM and TEM images show the SnO<sub>2</sub> nanocrystals uniformly mixed between the layers of graphene (Fig. 13c,d). Due to the amount of void space, the SnO<sub>2</sub> nanoparticles have room to expand upon the lithium intercalation (Fig. 13b). This results in the excellent cycle ability of this material. This graphene/SnO<sub>2</sub> composite was

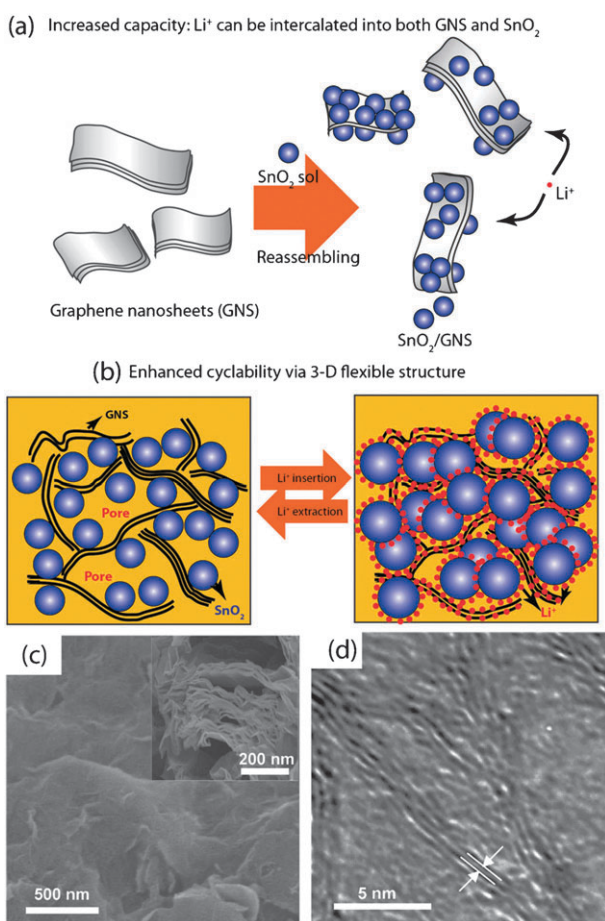


**Fig. 13** (a), (b) Schematic illustration for the synthesis and resulting structure of SnO<sub>2</sub>/GNS (c) SEM and (d) TEM images of SnO<sub>2</sub>/GNS. Adapted and reprinted with permission from ref. 117. Copyright 2009 American Chemical Society.

able to show an initial reversible capacity of  $810\text{ mAh/g}$  that only decreased to  $570\text{ mAh/g}$  after 30 cycles.

Wang *et al.* reported the growth of nanocrystalline TiO<sub>2</sub>, rutile and anatase, with graphene. This composite material showed significantly enhanced Li-ion insertion/extraction at high charge/discharge rates into the TiO<sub>2</sub>.<sup>118</sup> For example, at a high  $30\text{ C}$  (2 min charge/discharge) rate the rutile and anatase TiO<sub>2</sub> showed a capacity of  $87\text{ mAh/g}$  and  $96\text{ mAh/g}$  respectively.

Graphene/polyaniline composites have also been reported as flexible electrode materials for supercapacitors.<sup>119–121</sup> The graphene not only increases the electrical conductivity of the polymer, but can also increase its mechanical stability. The results of these studies showed heightened specific capacitances, better cycle abilities, and increased flexibility of these graphene/polyaniline composites over their pristine polyaniline counterparts.

Wang *et al.* reported single crystal hexagonal Co(OH)<sub>2</sub> nanoplates coated on graphene for supercapacitor applications. This composite displayed a very impressive specific capacitance of  $1335\text{ F/g}$  at a charge/discharge current density of  $2.8\text{ A/g}$ .<sup>122</sup>

Other types of 2-D heterogeneous nanostructures based on nanobelts, nanoflakes, nanodisks and nanosheets have also been investigated for their electrochemical energy storage properties.<sup>123–128</sup> For instance, Hassan *et al.* reported carbon-coated MoO<sub>3</sub> nanobelts as anode materials for lithium-ion batteries.<sup>124</sup> These composite nanobelts exhibited excellent cycle stability by maintaining a  $1064\text{ mAh/g}$  capacity after 50 cycles. Zheng *et al.* prepared carbon-nanotube/cobalt oxyhydroxide nanoflake multilayered films, which were shown to exhibit an excellent electrochemical specific capacitance of  $389\text{ F g}^{-1}$ .<sup>127</sup>

## 5. Three-dimensional (3-D) heterogeneous nanostructured networks

Although the ordered arrays of 1-D heterogeneous nanostructures are currently considered the most promising candidate to construct electrode materials with high energy densities at high power demands, a few disadvantages still exist. For example, when the 1-D nanomaterials are fabricated with high aspect ratios without interconnections, they tend to have a high electrical resistance due to their small diameters. In addition, it is difficult to maintain the structure's mechanical stability when they are grown exceedingly long with the upper part of the these 1-D nanomaterials tending to aggregate. Due to their structural interconnectivities, 3-D heterogeneous nanostructures can provide a solution to the above problems and are discussed in the following subsections: disordered/ordered 3-D porous nanostructures (section 5.1–5.3), complex hierarchy 3-D nanostructures (section 5.4) and future 3-D nanostructures (section 5.5).

### 5.1 Disordered porous 3-D nanostructured network: aerogel as an example

Aerogels or ambigels, a sol–gel-derived ultraporous solid, are of primary interest in this area because they exhibit a high surface area and provide continuous networks of  $10\text{ nm}$  nanowires and 3D-interconnected pores, which allow the easy

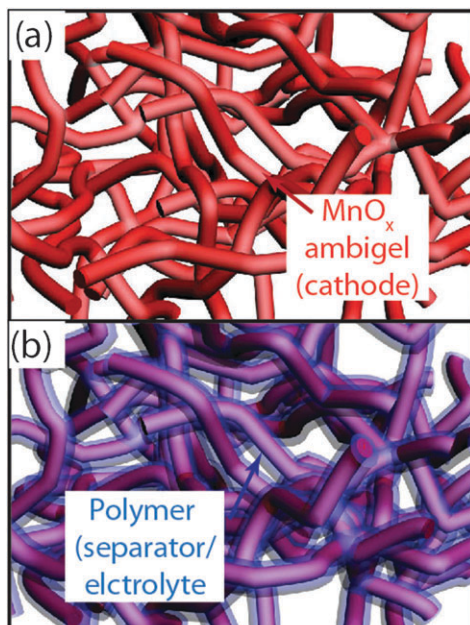
addition of energy dense materials to create heterogeneous nanostructures as electrode materials for electrochemical energy storage devices.<sup>129</sup>

Rolison's group has done intensive investigations on these aerogel-based heterogeneous nanoarchitectures as multi-functional battery materials.<sup>40,130–133</sup> In fact, an excellent review of three-dimensional nanomaterials and their applications in battery architectures for microdevices was written by Long *et al.*<sup>12</sup> The three-dimensionality of these nanomaterials allows for a high areal capacitance which is ideal for these small areal footprint devices.

In their research, they have reported a strategy to stabilize  $\text{MnO}_2$  ambigels in aqueous acid by electrodepositing a conformal coating of protective polymer, *o*-phenylenediamine.<sup>131</sup> This polymer coating not only protects the manganese oxide structure but can serve as a separator between the cathode and anode as well as contain the electrolyte for microbatteries (See Scheme 11).<sup>132</sup> The application of  $\text{MnO}_2$  as a supercapacitor material had been limited to neutral or slightly basic electrolytes; however, these heterogeneous organic-inorganic 3-D nanohybrids can be electrochemically cycled in aqueous acid electrolytes.

This same group has also reported the synthesis of a conformal layer of amorphous  $\text{MnO}_2$  onto carbon aerogels by a simple self-limiting reaction with an aqueous permanganate solution (Fig. 14a).<sup>130,133</sup>

The  $\text{MnO}_2$  coating increased the capacitance of the carbon nanofoam while maintaining its high-rate electrochemical performance due to the porous nature of the carbon network (Fig. 14b). The  $\text{MnO}_2$ -carbon composites produced a high areal capacitance of  $1.5 \text{ F cm}^{-2}$  and have possible applications as an on-chip power source for MEMS devices.



**Scheme 11** The conformal deposition of a separator/polymer phase over a high-surface area 3D electrode made of manganese oxide ambigels. Adapted and reprinted with permission from ref. 132. Copyright 2007 American Chemical Society.

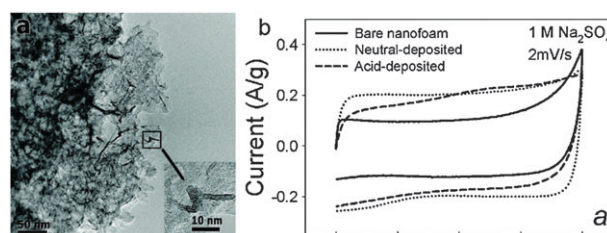


**Fig. 14** (a) TEM image of 240 min neutral-deposited  $\text{MnO}_2$ -carbon, (b) Cyclic voltammograms for bare carbon nanofoam, 240 min acid-deposited  $\text{MnO}_2$ -carbon nanofoam, and 240 min neutral deposited  $\text{MnO}_2$ -carbon nanofoam at  $2 \text{ mV s}^{-1}$ . Adapted and reprinted with permission from ref. 130. Copyright 2007 American Chemical Society.

Doherty *et al.* infiltrated a porous carbon monolith with  $\text{LiFePO}_4$  precursors and then thermally treated it. This 3-D  $\text{LiFePO}_4$ /carbon composite structure was able to achieve 82% ( $140 \text{ mAh g}^{-1}$ ) of the theoretical capacity of  $\text{LiFePO}_4$  at a 0.1C discharge rate and a large  $100 \text{ mAh/g}$  capacity at a high 5 C discharge rate.<sup>134</sup>

## 5.2 Three-dimensional ordered mesoporous materials

Highly ordered mesoporous carbons exhibit a high conductivity as well as a uniform pore diameter, a very high pore volume and an interconnected porous structure, which ensures an even distribution of electrolyte in contact with the electrode surface. They have been recently utilized by loading electroactive materials for electrochemical energy storage applications.<sup>135–140</sup>

For example, Ji *et al.* have established a nanostructured carbon–sulfur composite that was modified with the polymer PEG.<sup>135</sup> The sulfur insulating material is well-contacted to the conductive carbon matrix permitting the easy flow of electrons to the electroactive material (Fig. 15a–c). The carbon framework acts as a conductive substrate and inhibits the loss of sulfur to the electrolyte, while the polymer coating prevents the diffusion of the polysulfide units away from the cathode. This composite material reached nearly 80% ( $1320 \text{ mAh g}^{-1}$ ) of the theoretical capacity of sulfur (Fig. 15c) at a reasonably high charge/discharge rate of  $168 \text{ mA/g}$ .

Other lithium battery materials such as tin,<sup>138</sup> tin oxide,<sup>136</sup> silicon<sup>139</sup> have also been loaded onto mesoporous carbons to form composite nanomaterials with enhanced electrochemical properties.

Wang *et al.* has reported the growth of ordered whisker-like polyaniline on the surface of mesoporous carbon. The PANI/mesoporous carbon composite exhibited a very high specific capacitance of  $900 \text{ F g}^{-1}$  at a charge-discharge current density of  $0.5 \text{ A g}^{-1}$ .<sup>137</sup>

## 5.3 Three-dimensional ordered macroporous materials

Three-dimensionally ordered macroporous (3DOM) materials are composed of well-interconnected pore and wall structures with wall thicknesses of only a few tens of nanometers, which can enhance the rate performance of lithium-ion secondary batteries. The large pores in the 3DOM can be used as chambers to load other electroactive materials to increase the energy density of the 3DOM carbon. For example, Lee *et al.* synthesized tin oxide nanoparticles onto the surface of 3DOM carbon by thermally decomposing tin sulfate (Fig. 16). This composite displayed an

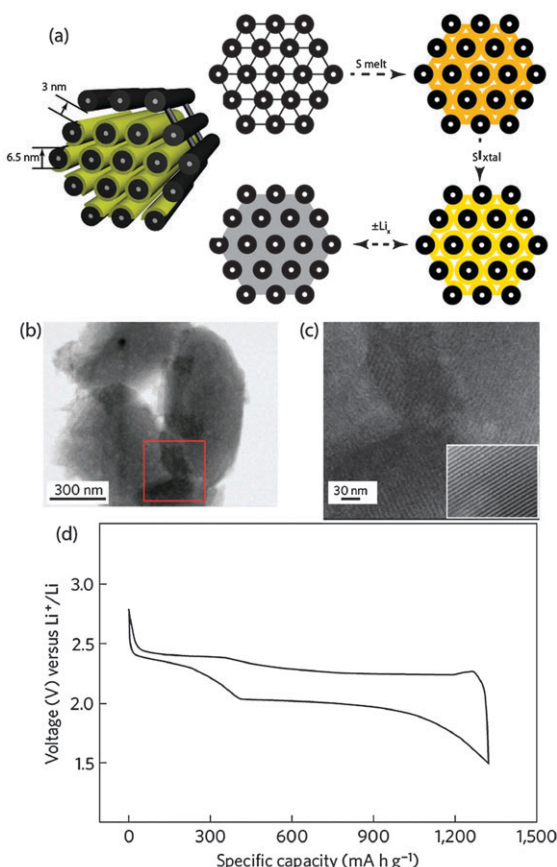


**Fig. 15** (a) Schematic diagram showing the synthesis of a sulfur mesoporous carbon composite and the strategy of pore-filling to adjust for volume expansion/contraction. (b) CMK-3/S-155 composite particle. (c) Image inset corresponding to the area outlined by the red square in (d) galvanostatic discharge–charge profile of PEG-modified CMK-3/S-155 recorded at room temperature at a current density of 168 mA g<sup>-1</sup>. Adapted and reprinted with permission from ref. 135. Copyright 2009 Macmillan Publishers Limited.

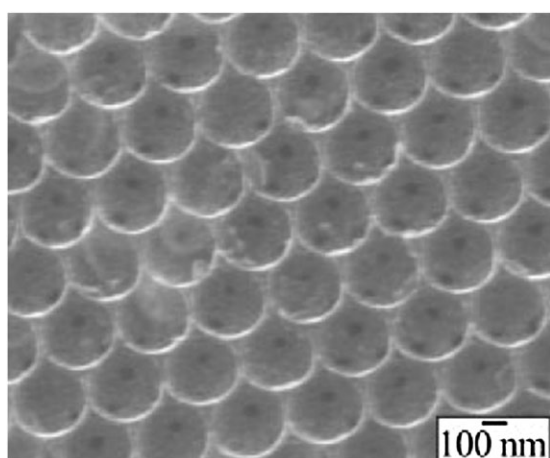


**Fig. 16** SEM image of tin oxide nanoparticles coated on the surface of 3DOM carbon. Adapted and reprinted with permission from ref. 141. Copyright 2005 Wiley-VCH.

increasing specific capacity from 299 to 348 mAh g<sup>-1</sup> at a charge/discharge current density of 15.2 mA g<sup>-1</sup>.<sup>141</sup>

Zhang *et al.* prepared conducting polymer-macroporous carbon composite electrode material by the deposition of a thin layer of polyaniline (PANI) on the surface of the 3DOM.<sup>142</sup> A specific capacitance of 1490 F/g was observed for the deposited PANI in the composite electrode.

#### 5.4 Other complex hierarchical 3-D heterogeneous nanostructures

More complex hierarchical 3-D heterogeneous nanostructures assembled by lower level nanoscaled building blocks have been proposed and have proved to be promising electrode materials for electrochemical energy storage.

For example, Magasinski *et al.* reported high performance lithium ion anodes based on a bottom-up 3-D synthesis approach. First, Si nanoparticles are deposited onto branched carbon-black nanoparticles by a CVD process. Then during an atmospheric pressured CVD deposition of C, the Si-coated carbon-black particles are self-assembled into spherical shaped granules (Fig. 17a and b).<sup>143</sup> This composite obtained a high capacity of 1950 mAh g<sup>-1</sup> with a high rate capability (Fig. 17c). Such high capacity was attributed to the aperiodic porous network consisting of disordered granules.

Wang *et al.* reported the synthesis of 3D aperiodic hierarchical porous graphitic carbon as a potential electrode material for high power electrochemical capacitor applications.<sup>144,145</sup> These 3D porous nanoparticles consisted of a core with macropores to act as ion-buffering reservoirs, a mesoporous wall to increase ion conductivity, and micropores to enhance electronic conductivity while increasing the electric double layer (Fig. 18a). The experimental results observed have shown higher energy densities at high charge/discharge rates than previously researched high surface area carbons (Fig. 18b).

RuO<sub>2</sub> nanoparticles have been used as conductive wires to connect electroactive materials such as LiFePO<sub>4</sub><sup>146</sup> and TiO<sub>2</sub><sup>147</sup> to form heterogeneously mixed conducting matrices,

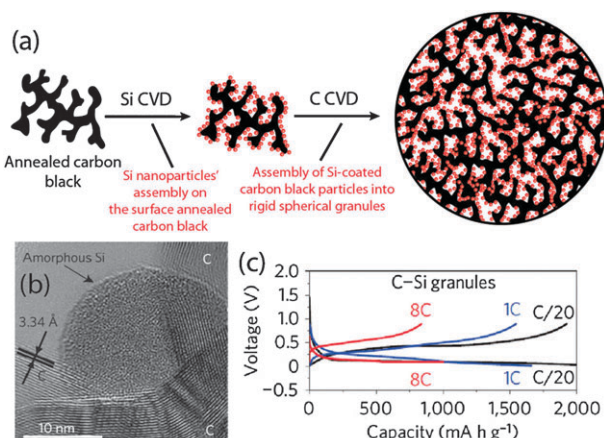


**Fig. 17** (a) Schematic of Si-C nanocomposite granule formation through a hierarchical bottom-up assembly. (b) TEM image showing the highly ordered graphitic structure of the carbon-black surface with a (002) interplanar spacing of 3.34 Å and the amorphous structure of Si. (c) Galvanostatic charge–discharge profiles of the C–Si granule electrode at different charge/discharge rates. Adapted and reprinted with permission from ref. 143. Copyright 2010 Nature Publishing Group.

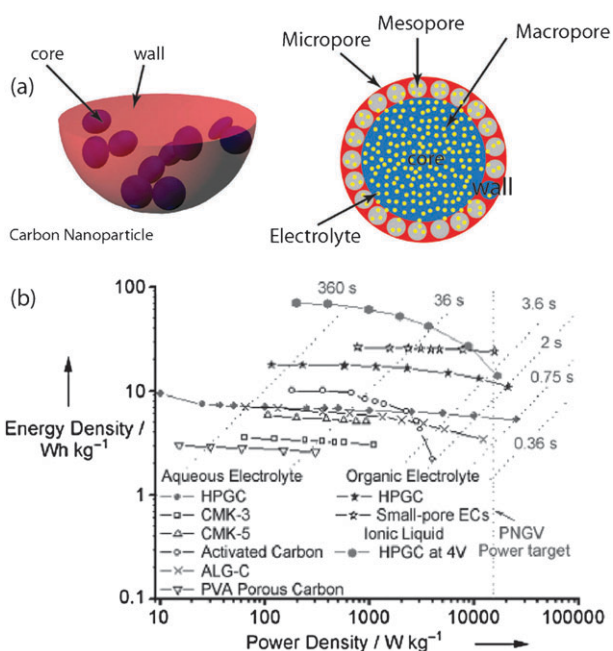


**Fig. 18** (a) Schematic representation of the 3D hierarchical porous texture (b) Ragone plot showing the position of the HPGC material relative to other forms of carbon materials. Adapted and reprinted with permission from ref. 144 and 145. Copyright 2008, 2009 Wiley-VCH.

which are shown to improve electrode performance by enhancing the composite materials conductivity.

Hierarchical nanowire composites formed by interpenetrated carbon nanotubes and vanadium pentoxide ( $V_2O_5$ ) nanowires networks have been reported by Chen *et al.*, this composite was shown to be an excellent electrode material for supercapacitors with high energy densities and high power capabilities.<sup>148</sup>

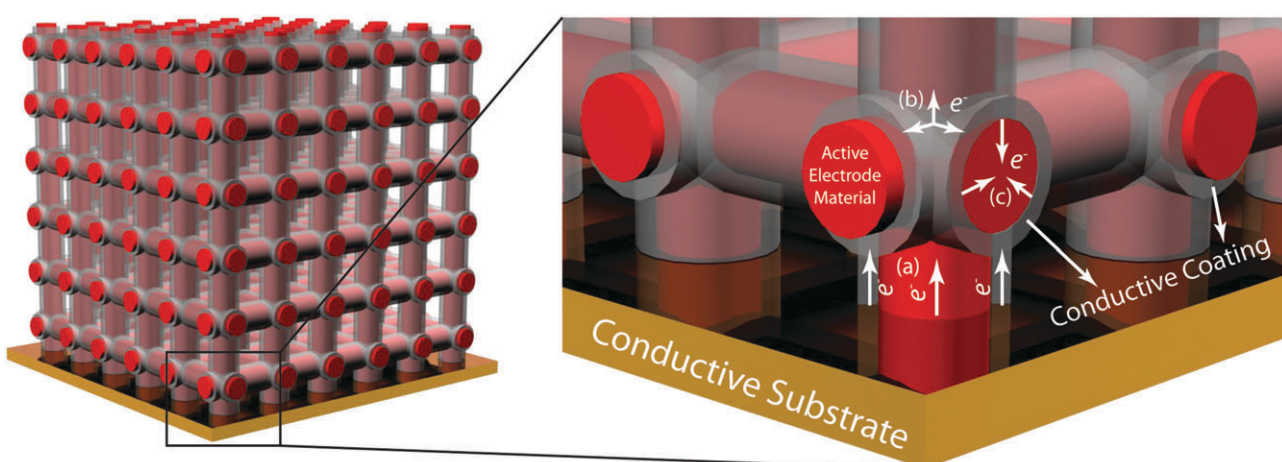
### 5.5 Future 3-D heterogeneous nanostructured electrode

The previous four subsections (5.1–5.4) have shown excellent examples of how 3-D heterogeneous porous nanostructures can improve electrochemical energy storage

devices.<sup>12,39,40,130–143,145–151</sup> However, optimizing the pore structures such as controlling the pore size and the pore order remains a challenge. Controlling these could help these materials to achieve their best electrochemical performance as electroactive materials. Here, we tend to propose a future 3-D heterogeneous nanostructures which is shown in Scheme 12.

This proposed structure is composed of well ordered 3-D interconnected pores and a well ordered 3-D interconnected electroactive nanomaterial with a conformal conductive coating layer. There are a few advantages of this proposed structure. (1) The interconnectivity of the electrode material provides a 3-D continuous electron pathway (Scheme 12) and can exhibit the same mechanical robustness as its bulk counterpart, while the interconnected ordered pores allow for the electrolyte to penetrate and evenly contact the electrode material (If the pore size is too large it will lower the volumetric energy of this electrode, while if it is too small it will cause increase in pore resistance to the electrolyte resulting in an incomplete wetting of the pores). (2) The 3-D interconnected coating of conductive material not only facilitates fast electron transfer into the 3-D continuous framework (Scheme 12), but also due to its conformality allows for electrons to be directly transported to the core electrode materials (Scheme 12). (3) By virtue of the material being directly contacted with a substrate that is conductive, electrons can easily transfer from the conductive substrate to the electroactive core-material as well as to the conductive shell that coats the material (Scheme 12).

One possible draw back for this 3-D architected electrode is that the electrode strain stress can not be released as efficiently as in the 1-D nanostructured arrays because all the materials are interconnected with less freedom for expansion/contraction during lithium insertion/deinsertion. In order to overcome this obstacle, high mechanical flexibility and resiliency is required for the conductive coating in order to accommodate for the volume changes of the nanowires. Another option is to reverse the core and shell materials resulting in an interconnected 3-D nanostructured current collector coated with thin layer of electroactive material.



**Scheme 12** Future 3-D heterogeneous nanostructured electrode.

**Table 1** The advantages and features of heterogeneous nanostructures with various nanodimensionalities as well as selected examples and their specific electrochemical performance

Category	Subcategory	Principle features	Advantages	Selected examples	Electrochemical properties
0-D	Core-shell nanoparticles	Core energy dense nanoparticles coated with thin conductive shells	The core material provides the energy density while the shell supplies electrical conductivity, prevents aggregation, improves chemical stability, and buffers the stress associated with any volume change of the core upon cycling.	LiFePO <sub>4</sub> core/carbon shell <sup>41</sup> Sn <sub>0.9</sub> Si <sub>0.1</sub> core/carbon shell <sup>51</sup> Fe <sub>3</sub> O <sub>4</sub> core/carbon shell <sup>70</sup>	169 mAh/g at 0.6 C rate 90 mAh/g at 60 C rate 95% Retention over 1100 cycles 964 mAh/g at 0.3 C rate 85% Retention over 50 cycles 745 mAh/g at 0.2 C rate 190 mAh/g at 5 C rate 88% Retention over 80 cycles 687 mAh/g at 0.25 C rate 290 mAh/g at 5 C rate 76% Retention over 200 cycles 1107 mAh/g at 0.25 C rate 200 mAh/g at 5 C Rate
	Small nanoparticles dispersed and confined in the matrix of larger conductive nanoparticles	Small energy dense nanoparticles loaded into a matrix of larger, more conductive nanoparticles	The larger conductive nanoparticle matrix buffers any volume changes, allows fast electron and ion transfer, and prevents conglomerate of the small energy dense nanoparticles.	Sb nanoparticles in Al <sub>4</sub> C <sub>3</sub> /C matrix <sup>72</sup> ZnP <sub>2</sub> nanoparticles in carbon matrix <sup>73</sup> $\alpha$ -Fe <sub>2</sub> O <sub>3</sub> nanoparticles in hollow carbon nanosphere matrix <sup>74</sup>	1210 mAh/g at 0.1 C rate 722 mAh/g at 2 C rate Capacity increased during cycling
	Hollow nanosphere loaded with active nanoparticles	Nanoparticles with high energy density encapsulated in hollow conductive nanospheres	The hollow nanosphere provides a connective electron pathway for the nanoparticles, while the large void volume in the sphere helps prevent the nanoparticles from agglomerating, and effectively buffers stress associated with any volume change.	Sn nanoparticles encapsulated in hollow carbon nanospheres <sup>76</sup> SnO <sub>2</sub> nanoparticles encapsulated in hollow carbon nanospheres <sup>78</sup> SnO <sub>2</sub> mesoporous hollow nanospheres coated inside and out with carbon <sup>79</sup> SnO <sub>2</sub> nanoparticles loaded on a carbon nanotube network <sup>45</sup> Si nanoparticles loaded on TiSi <sub>2</sub> nanonets <sup>90</sup> Si nanoparticles embedded in carbon nanofiber matrix <sup>91</sup>	800 mAh/g at 0.2 C rate 69% Retention over 100 cycles 468 mAh/g at 0.2 C rate 91% Retention over 60 cycles 983 mAh/g charge capacity at 100 mA/g rate 473 mAh/g over 50 cycles 850 mAh/g at 0.1 C 100% Retention over 65 cycles >1000 mAh/g at 8400 mA/g 99% Retention over 100 Cycles (Variable Depending on Pre-cursor Ratio PAN/15 wt% Si:886 mAh/g at 50 mA/g 51% Retention over 50 Cycles
1-D	Disordered network of 1-D heterogeneous nanostructures	Nanowires or nanotubes irregularly oriented and connected to form a disordered network onto which electroactive materials can be deposited	The 1-D Nanostructure network provides a continuous electron pathway for better kinetics, a high surface area substrate for higher ion flux, and buffer volume between structures to alleviate any stress during cycling.	MnO <sub>2</sub> core/PEDOT shell coaxial nanowires <sup>46</sup> MnO <sub>2</sub> nanoparticles dispersed in PEDOT nanowires <sup>44</sup> Fe <sub>3</sub> O <sub>4</sub> deposited on Cu nanowires <sup>34</sup>	210 F/g at 5 mA/cm <sup>2</sup> 185 F/g at 25 mA/cm <sup>2</sup> 250 F/g at 5 mA/cm <sup>2</sup> >200 F/g at 25 mA/cm <sup>2</sup> 90% Retention over 500 cycles ~800 mAh/g at 0.25 C rate ~640 mAh/g at 8 C rate Capacity increases upon cycling
	Well ordered arrays of 1-D nanostructured materials	Arrays of 1-D heterogeneous nanostructures oriented in the same axial direction	There is no need for extra binders or conductive additives as each nanostructure is directly attached to the current collector. The void volume between the neighbouring 1-D nanomaterials can allow for easy penetration of the electrolyte resulting in a high ion flux and can also accommodate a materials volume change during cycling.	RuO <sub>2</sub> deposited inside porous PEDOT nanotubes <sup>32</sup>	664 F/g at 5 mA/cm <sup>2</sup> 530 F/g at 25 mA/cm <sup>2</sup>

**Table 1 (continued)**

Category	Subcategory	Principle features	Advantages	Selected examples	Electrochemical properties
2-D	Nanosheets or nanofilms	Heterogeneous nanofilms, nanobelts, or nanoplates	For heterogeneous 2-D nanostructures, all material is within a few nanometers from either the electrolyte or a conductive material for straightforward electron and ion transfer resulting in high energy densities at high power demands.	SnO <sub>2</sub> nanoparticles deposited on graphene nanosheets <sup>117</sup> Rutile or anatase TiO <sub>2</sub> nanoparticles deposited on graphene sheets <sup>118</sup>	810 mAh/g at 50 mA/g 70% Retention over 30 cycles Rutile TiO <sub>2</sub> /graphene: 87 mAh/g at 30 °C rate >90% Retention over 100 cycles Anatase TiO <sub>2</sub> /graphene: 96 mAh/g at 30°C rate >90% Retention over 100 cycles
3-D	Disordered porous 3-D nanostructured network	Continuous networks of conductive materials with 3-D disordered pores, which are coated with energy dense materials.	High surface area and continuous networks of interconnected pores allow electrolyte access deep into the material increasing the amount of electroactive material.	Ni(OH) <sub>2</sub> nanocrystals grown on graphene sheets <sup>122</sup>	935 F/g at 2.8 A/g 667 F/g at 45.7 A/g ~100% Retention over 2000 cycles
	Three-dimensional ordered mesoporous materials	Mesoporous carbons with 3-D ordered pores onto which energy dense material can be deposited	The carbon provides a high conductivity as well as a uniform pore diameter, a very high pore volume and an interconnected porous structure, which ensures an even distribution of electrolyte in contact with the energy dense material.	Carbon nanofoam with MnO <sub>2</sub> conformally coated on pore walls <sup>133</sup> Meso/macroporous carbon monolith with LiFePO <sub>4</sub> lining the pores <sup>134</sup> Ordered mesoporous carbon with sulfur lining the pores <sup>135</sup> Tin-based oxides infiltrating the pores of ordered mesoporous carbon <sup>136</sup> Polyaniline whiskers grown On surface of ordered mesoporous carbon <sup>137</sup>	146 mAh/g at 250 mA/g 135 mAh/g at 1000 mA/g 140 mAh/g at 1 C 100 mAh/g at 5 C 1320 mAh/g at 0.1 C rate ~79% Retention over 20 cycles 515 mAh/g at 0.5 mA/cm <sup>2</sup> 43% Retention over 30 cycles 900 F/g at 500 mA/g 768 F/g at 5000 mA/g 95% Retention over 3000 cycles
	Future 3-D heterogeneous nanostructured electrode	Macroporous carbons with large 3-D ordered pores onto which energy dense material can be deposited	Carbon contains interconnected pores and wall structures with thicknesses of only a few tens of nanometers, which provide high ion flux and short ion diffusion lengths.	348 mAh/g at 15.2 mA/g ~202 mAh/g at 90.9 mA/g	352 F/g at 500 mA/g 278 F/g at 1000 mA/g 79% Retention over 1000 cycles 1950 mAh/g at 0.05 °C rate 870 mAh/g at 8 °C rate
	Other complex hierarchical 3-D heterogeneous nanostructures	Energy dense nanoparticles coated on the surface of disordered 3-D conductive porous networks	Morphology provides facile electron and ion access to the energy dense nanoparticles, while the ultra high surface area of the nanoparticles results in a large energy density.	~80 Wh/kg at 0.2 kW/kg 10.8 Wh/kg at 21 kW/kg	The interconnectivity of the energy storage material provides continuous electron pathways as well as high mechanical strength for great cycle life. The well ordered interconnected pores allow for deep penetration of the electrolyte, while the conductive coating facilitates fast electron transfer into the 3-D continuous framework for high rate capabilities.

## 6. Conclusion and outlook

In this review, we have summarized the recent advances of using heterogeneous nanostructures as electrode materials for electrochemical energy storage devices, such as lithium ion batteries or supercapacitors. Table 1 displays the properties and advantages of each nanodimensionality along with some selected examples and their electrochemical properties.

The heterogeneous nanostructured materials are composed of multi-nanocomponents, each tailored to address different requirements (*e.g.*, high energy density, high conductivity, excellent mechanical stability, *etc.*). The resulting composite materials have been shown to exhibit synergic properties, allowing the energy dense materials to approach their theoretical potential in electrochemical energy storage devices (*e.g.* high energy density at high power density).

We have discussed heterogeneous nanomaterials based on their structural complexity, *i.e.* from simplest 0-dimensional (0-D) to the most complex 3-dimensional (3-D) nanostructured network. Ordered arrays of 1-D heterogeneous nanomaterials are considered to be the most promising candidate for highly efficient electrochemical energy storage devices, and thus they are the most discussed heterogeneous nanostructure in this article. Certainly, it is realized that all current heterogeneous nanostructures have their own drawbacks. For example, promising 1-D nanostructures can become mechanically unstable when they are grown excessively long in the axial direction. This will limit their use as on-chip power sources for MEMS devices and other applications where the areal footprint is at a premium and a high areal energy density is needed. This limitation could be overcome by our proposed 3-D nanostructured electrode with its interconnected electroactive nanomaterial which can be seen as adding more energy density between the 1-D nanostructures and can be grown at longer lengths perpendicular to the current collector axis without compromising its mechanical stability.

It is imperative that we as scientists put considerable effort into developing more technologically advanced nano-architectures to fulfil the future requirements of electrochemical energy storage devices.

## Acknowledgements

The work was supported by Laboratory for Physical Sciences and also supported as part of the Science of Precision Multifunctional Nanostructures for Electrical Energy Storage, an Energy Frontier Research Centre funded by the US Department of Energy, Office of Science, Office of Basic Energy Sciences under Award Number DESC0001160 (J.D., S.B.L.). S.B.L. thanks the WCU program funded by the KOSEF under the MEST (grant number: R31-2008-000-10071-0).

## Notes and references

- M. Winter and R. J. Brodd, *Chem. Rev.*, 2004, **104**, 4245–4269.
- J. M. Tarascon and M. Armand, *Nature*, 2001, **414**, 359–367.
- A. S. Arico, P. Bruce, B. Scrosati, J. M. Tarascon and W. Van Schalkwijk, *Nat. Mater.*, 2005, **4**, 366–377.
- P. G. Bruce, B. Scrosati and J. M. Tarascon, *Angew. Chem., Int. Ed.*, 2008, **47**, 2930–2946.
- F. Cheng, Z. Tao, J. Liang and J. Chen, *Chem. Mater.*, 2008, **20**, 667–681.
- B. L. Ellis, K. T. Lee and L. F. Nazar, *Chem. Mater.*, 2010, **22**, 691–714.
- Y. G. Guo, J. S. Hu and L. J. Wan, *Adv. Mater.*, 2008, **20**, 2878–2887.
- J. B. Goodenough and Y. Kim, *Chem. Mater.*, 2010, **22**, 587–603.
- M. G. Kim and J. Cho, *Adv. Funct. Mater.*, 2009, **19**, 1497–1514.
- H. Li, Z. X. Wang, L. Q. Chen and X. J. Huang, *Adv. Mater.*, 2009, **21**, 4593–4607.
- C. Liu, F. Li, L. P. Ma and H. M. Cheng, *Adv. Mater.*, 2010, **22**, E28–E62.
- J. W. Long, B. Dunn, D. R. Rolison and H. S. White, *Chem. Rev.*, 2004, **104**, 4463–4492.
- P. Simon and Y. Gogotsi, *Nat. Mater.*, 2008, **7**, 845–854.
- M. S. Whittingham, *Chem. Rev.*, 2004, **104**, 4271–4301.
- M. Winter, J. O. Besenhard, M. E. Spahr and P. Novak, *Adv. Mater.*, 1998, **10**, 725–763.
- L. L. Zhang and X. S. Zhao, *Chem. Soc. Rev.*, 2009, **38**, 2520–2531.
- K. S. Kang, Y. S. Meng, J. Breger, C. P. Grey and G. Ceder, *Science*, 2006, **311**, 977–980.
- R. F. Service, *Science*, 2006, **313**, 902–902.
- D. N. Futaba, K. Hata, T. Yamada, T. Hiraoka, Y. Hayamizu, Y. Kakudate, O. Tanaike, H. Hatori, M. Yumura and S. Iijima, *Nat. Mater.*, 2006, **5**, 987–994.
- N. A. Kaskhedikar and J. Maier, *Adv. Mater.*, 2009, **21**, 2664–2680.
- T. Song, J. L. Xia, J. H. Lee, D. H. Lee, M. S. Kwon, J. M. Choi, J. Wu, S. K. Doo, H. Chang, W. Il Park, D. S. Zang, H. Kim, Y. G. Huang, K. C. Hwang, J. A. Rogers and U. Paik, *Nano Lett.*, 2010, **10**, 1710–1716.
- C. K. Chan, H. L. Peng, G. Liu, K. McElwraith, X. F. Zhang, R. A. Huggins and Y. Cui, *Nat. Nanotechnol.*, 2008, **3**, 31–35.
- Y. Yu, L. Gu, C. B. Zhu, S. Tsukimoto, P. A. van Aken and J. Maier, *Adv. Mater.*, 2010, **22**, 2247.
- Z. G. Yang, D. Choi, S. Kerisit, K. M. Rosso, D. H. Wang, J. Zhang, G. Graff and J. Liu, *J. Power Sources*, 2009, **192**, 588–598.
- D. Deng, M. G. Kim, J. Y. Lee and J. Cho, *Energy Environ. Sci.*, 2009, **2**, 818–837.
- G. Amatucci and J. M. Tarascon, *J. Electrochem. Soc.*, 2002, **149**, K31–K46.
- N. C. Li, C. J. Patrissi, G. L. Che and C. R. Martin, *J. Electrochem. Soc.*, 2000, **147**, 2044–2049.
- Y. Wang and G. Z. Cao, *Adv. Mater.*, 2008, **20**, 2251–2269.
- B. Kang and G. Ceder, *Nature*, 2009, **458**, 190–193.
- A. K. Padhi, K. S. Nanjundaswamy and J. B. Goodenough, *J. Electrochem. Soc.*, 1997, **144**, 1188–1194.
- M. S. Kim, T. W. Lee and J. H. Parka, *J. Electrochem. Soc.*, 2009, **156**, A584–A588.
- R. Liu, J. Duay, T. Lane and S. B. Lee, *Phys. Chem. Chem. Phys.*, 2010, **12**, 4309–4316.
- W. Sugimoto, K. Yokoshima, Y. Murakami and Y. Takasu, *Electrochim. Acta*, 2006, **52**, 1742–1748.
- L. Taberna, S. Mitra, P. Poizot, P. Simon and J. M. Tarascon, *Nat. Mater.*, 2006, **5**, 567–573.
- K. W. Chung, K. B. Kim, S. H. Han and H. Lee, *Electrochim. Solid-State Lett.*, 2005, **8**, A259–A262.
- C. J. Xu, F. Y. Kang, B. H. Li and H. D. Du, *J. Mater. Res.*, 2010, **25**, 1421–1432.
- B. E. Conway, *Electrochemical Supercapacitors: Scientific Fundamentals and Technological Applications*, Plenum Press, New York, 1999.
- H. S. Zhou, D. L. Li, M. Hibino and I. Honma, *Angew. Chem., Int. Ed.*, 2005, **44**, 797–802.
- K. M. Shaju and P. G. Bruce, *Adv. Mater.*, 2006, **18**, 2330–2334.
- D. R. Rolison, R. W. Long, J. C. Lytle, A. E. Fischer, C. P. Rhodes, T. M. McEvoy, M. E. Bourga and A. M. Lubers, *Chem. Soc. Rev.*, 2009, **38**, 226–252.
- Y. G. Wang, Y. R. Wang, E. J. Hosono, K. X. Wang and H. S. Zhou, *Angew. Chem., Int. Ed.*, 2008, **47**, 7461–7465.

- 42 L. J. Fu, H. Liu, C. Li, Y. P. Wu, E. Rahm, R. Holze and H. Q. Wu, *Solid State Sci.*, 2006, **8**, 113–128.
- 43 T. Fang, J. G. Duh and S. R. Sheen, *J. Electrochem. Soc.*, 2005, **152**, A1701–A1706.
- 44 R. Liu, J. Duay and S. B. Lee, *ACS Nano*, 2010, **4**, 4299–4307.
- 45 H. X. Zhang, C. Feng, Y. C. Zhai, K. L. Jiang, Q. Q. Li and S. S. Fan, *Adv. Mater.*, 2009, **21**, 2299–2304.
- 46 R. Liu and S. B. Lee, *J. Am. Chem. Soc.*, 2008, **130**, 2942–2943.
- 47 H. Zhang, G. P. Cao, Z. Y. Wang, Y. S. Yang, Z. J. Shi and Z. N. Gu, *Nano Lett.*, 2008, **8**, 2664–2668.
- 48 S. Cahen, R. Janot, L. Laffont-Dantras and J. M. Tarascon, *J. Electrochem. Soc.*, 2008, **155**, A512–A519.
- 49 K. Saravanan, M. V. Reddy, P. Balaya, H. Gong, B. V. R. Chowdari and J. J. Vittal, *J. Mater. Chem.*, 2009, **19**, 605–610.
- 50 D. W. Kim, I. S. Hwang, S. J. Kwon, H. Y. Kang, K. S. Park, Y. J. Choi, K. J. Choi and J. G. Park, *Nano Lett.*, 2007, **7**, 3041–3045.
- 51 Y. Kwon, H. Kim, S. G. Doo and J. H. Cho, *Chem. Mater.*, 2007, **19**, 982–986.
- 52 H. M. Xie, R. S. Wang, J. R. Ying, L. Y. Zhang, A. F. Jalbout, H. Y. Yu, G. L. Yang, X. M. Pan and Z. M. Su, *Adv. Mater.*, 2006, **18**, 2609.
- 53 G. Armstrong, A. R. Armstrong, J. Canales and P. G. Bruce, *Chem. Commun.*, 2005, 2454–2456.
- 54 G. L. Che, B. B. Lakshmi, E. R. Fisher and C. R. Martin, *Nature*, 1998, **393**, 346–349.
- 55 C. C. Hu, K. H. Chang, M. C. Lin and Y. T. Wu, *Nano Lett.*, 2006, **6**, 2690–2695.
- 56 S. Il Cho and S. B. Lee, *Acc. Chem. Res.*, 2008, **41**, 699–707.
- 57 D. K. Kim, P. Muralidharan, H. W. Lee, R. Ruffo, Y. Yang, C. K. Chan, H. Peng, R. A. Huggins and Y. Cui, *Nano Lett.*, 2008, **8**, 3948–3952.
- 58 W. Y. Li, L. N. Xu and J. Chen, *Adv. Funct. Mater.*, 2005, **15**, 851–857.
- 59 X. X. Li, F. Y. Cheng, B. Guo and J. Chen, *J. Phys. Chem. B*, 2005, **109**, 14017–14024.
- 60 Y. G. Li, B. Tan and Y. Y. Wu, *Nano Lett.*, 2008, **8**, 265–270.
- 61 R. Liu, S. Il Cho and S. B. Lee, *Nanotechnology*, 2008, **19**, 215710.
- 62 K. T. Nam, D. W. Kim, P. J. Yoo, C. Y. Chiang, N. Meethong, P. T. Hammond, Y. M. Chiang and A. M. Belcher, *Science*, 2006, **312**, 885–888.
- 63 M. Nishizawa, K. Mukai, S. Kuwabata, C. R. Martin and H. Yoneyama, *J. Electrochem. Soc.*, 1997, **144**, 1923–1927.
- 64 M. S. Park, G. X. Wang, Y. M. Kang, D. Wexler, S. X. Dou and H. K. Liu, *Angew. Chem., Int. Ed.*, 2007, **46**, 750–753.
- 65 A. L. M. Reddy, M. M. Shajumon, S. R. Gowda and P. M. Ajayan, *Nano Lett.*, 2009, **9**, 1002–1006.
- 66 C. R. Sides, F. Croce, V. Y. Young, C. R. Martin and B. Scrosati, *Electrochem. Solid-State Lett.*, 2005, **8**, A484–A487.
- 67 Y. Sharma, N. Sharma, G. V. S. Rao and B. V. R. Chowdari, *Adv. Funct. Mater.*, 2007, **17**, 2855–2861.
- 68 Y. S. Hu, L. Kienle, Y. G. Guo and J. Maier, *Adv. Mater.*, 2006, **18**, 1421–1426.
- 69 M. G. Kim, S. Lee and J. Cho, *J. Electrochem. Soc.*, 2009, **156**, A89–A94.
- 70 W. M. Zhang, X. L. Wu, J. S. Hu, Y. G. Guo and L. J. Wan, *Adv. Funct. Mater.*, 2008, **18**, 3941–3946.
- 71 Y. Kwon and J. Cho, *Chem. Commun.*, 2008, 1109–1111.
- 72 C. M. Park and H. J. Sohn, *Chem. Mater.*, 2008, **20**, 3169–3173.
- 73 C. M. Park and H. J. Sohn, *Chem. Mater.*, 2008, **20**, 6319–6324.
- 74 S. L. Chou, J. Z. Wang, D. Wexler, K. Konstantinov, C. Zhong, H. K. Liu and S. X. Dou, *J. Mater. Chem.*, 2010, **20**, 2092–2098.
- 75 L. Chen, C. Z. Yuan, B. Gao, S. Y. Chen and X. G. Zhang, *J. Solid State Electrochem.*, 2009, **13**, 1925–1933.
- 76 W. M. Zhang, J. S. Hu, Y. G. Guo, S. F. Zheng, L. S. Zhong, W. G. Song and L. J. Wan, *Adv. Mater.*, 2008, **20**, 1160–1165.
- 77 K. T. Lee, Y. S. Jung and S. M. Oh, *J. Am. Chem. Soc.*, 2003, **125**, 5652–5653.
- 78 Y. Wang, F. B. Su, J. Y. Lee and X. S. Zhao, *Chem. Mater.*, 2006, **18**, 1347–1353.
- 79 X. W. Lou, D. Deng, J. Y. Lee and L. A. Archer, *Chem. Mater.*, 2008, **20**, 6562–6566.
- 80 Y. Hou, Y. Cheng, T. Hobson and J. Liu, *Nano Lett.*, 2010, **10**, 2727–2733.
- 81 W. X. Chen, J. Y. Lee and Z. L. Liu, *Carbon*, 2003, **41**, 959–966.
- 82 G. Chen, Z. Y. Wang and D. G. Xia, *Chem. Mater.*, 2008, **20**, 6951–6956.
- 83 E. Frackowiak, V. Khomenko, K. Jurewicz, K. Lota and F. Beguin, *J. Power Sources*, 2006, **153**, 413–418.
- 84 K. H. An, K. K. Jeon, J. K. Heo, S. C. Lim, D. J. Bae and Y. H. Lee, *J. Electrochem. Soc.*, 2002, **149**, A1058–A1062.
- 85 E. Raymundo-Pinero, V. Khomenko, E. Frackowiak and F. Beguin, *J. Electrochem. Soc.*, 2005, **152**, A229–A235.
- 86 L. F. Cui, Y. Yang, C. M. Hsu and Y. Cui, *Nano Lett.*, 2009, **9**, 3370–3374.
- 87 Y. J. Lee, H. Yi, W. J. Kim, K. Kang, D. S. Yun, M. S. Strano, G. Ceder and A. M. Belcher, *Science*, 2009, **324**, 1051–1055.
- 88 L. F. Cui, R. Ruffo, C. K. Chan, H. L. Peng and Y. Cui, *Nano Lett.*, 2009, **9**, 491–495.
- 89 J. Yan, E. Khoo, A. Sumboja and P. S. Lee, *ACS Nano*, 2010, **4**, 4247–4255.
- 90 S. Zhou, X. H. Liu and D. W. Wang, *Nano Lett.*, 2010, **10**, 860–863.
- 91 L. W. Ji and X. W. Zhang, *Carbon*, 2009, **47**, 3219–3226.
- 92 J. Li, L. Cui and X. G. Zhang, *Appl. Surf. Sci.*, 2010, **256**, 4339–4343.
- 93 P. Sen and A. De, *Electrochim. Acta*, 2010, **55**, 4677–4684.
- 94 C. R. Sides, N. C. Li, C. J. Patrissi, B. Scrosati and C. R. Martin, *Mrs Bulletin*, 2002, **27**, 604–607.
- 95 C. J. Patrissi and C. R. Martin, *J. Electrochem. Soc.*, 2001, **148**, A1247–A1253.
- 96 N. C. Li and C. R. Martin, *J. Electrochem. Soc.*, 2001, **148**, A164–A170.
- 97 N. C. Li, C. R. Martin and B. Scrosati, *J. Power Sources*, 2001, **97**, 240–243.
- 98 N. C. Li, C. R. Martin and B. Scrosati, *Electrochem. Solid-State Lett.*, 2000, **3**, 316–318.
- 99 C. J. Patrissi and C. R. Martin, *J. Electrochem. Soc.*, 1999, **146**, 3176–3180.
- 100 W. Wang and P. N. Kumta, *ACS Nano*, 2010, **4**, 2233–2241.
- 101 H. Lee, M. S. Cho, I. H. Kim, J. D. Nam and Y. Lee, *Synth. Met.*, 2010, **160**, 1055–1059.
- 102 J. Hassoun, S. Panero, P. Simon, P. L. Taberna and B. Scrosati, *Adv. Mater.*, 2007, **19**, 1632–1635.
- 103 Y. Wang, H. C. Zeng and J. Y. Lee, *Adv. Mater.*, 2006, **18**, 645–649.
- 104 H. Pan, C. K. Poh, Y. P. Feng and J. Y. Lin, *Chem. Mater.*, 2007, **19**, 6120–6125.
- 105 Y. S. Hu, X. Liu, J. O. Muller, R. Schlogl, J. Maier and D. S. Su, *Angew. Chem., Int. Ed.*, 2009, **48**, 210–214.
- 106 K. Takahashi, Y. Wang and G. Z. Cao, *J. Phys. Chem. B*, 2005, **109**, 48–51.
- 107 J. S. Ye, H. F. Cui, X. Liu, T. M. Lim, W. D. Zhang and F. S. Sheu, *Small*, 2005, **1**, 560–565.
- 108 M. Hughes, M. S. P. Shaffer, A. C. Renouf, C. Singh, G. Z. Chen, J. Fray and A. H. Windle, *Adv. Mater.*, 2002, **14**, 382–385.
- 109 A. Ghicov, M. Yamamoto and P. Schmuki, *Angew. Chem., Int. Ed.*, 2008, **47**, 7934–7937.
- 110 A. R. Armstrong, G. Armstrong, J. Canales, R. Garcia and P. G. Bruce, *Adv. Mater.*, 2005, **17**, 862.
- 111 H. Zhang, G. R. Li, L. P. An, T. Y. Yan, X. P. Gao and H. Y. Zhu, *J. Phys. Chem. C*, 2007, **111**, 6143–6148.
- 112 H. L. Zhang, F. Li, C. Liu and H. M. Cheng, *Nanotechnology*, 2008, **19**, 165606.
- 113 M. V. Reddy, T. Yu, C. H. Sow, Z. X. Shen, C. T. Lim, G. V. S. Rao and B. V. R. Chowdari, *Adv. Funct. Mater.*, 2007, **17**, 2792–2799.
- 114 J. W. Seo, J. T. Jang, S. W. Park, C. J. Kim, B. W. Park and J. W. Cheon, *Adv. Mater.*, 2008, **20**, 4269–4273.
- 115 E. Yoo, J. Kim, E. Hosono, H. Zhou, T. Kudo and I. Honma, *Nano Lett.*, 2008, **8**, 2277–2282.
- 116 M. D. Stoller, S. J. Park, Y. W. Zhu, J. H. An and R. S. Ruoff, *Nano Lett.*, 2008, **8**, 3498–3502.
- 117 S. M. Paek, E. Yoo and I. Honma, *Nano Lett.*, 2009, **9**, 72–75.
- 118 D. H. Wang, D. W. Choi, J. Li, Z. G. Yang, Z. M. Nie, R. Kou, D. H. Hu, C. M. Wang, L. V. Saraf, J. G. Zhang, I. A. Aksay and J. Liu, *ACS Nano*, 2009, **3**, 907–914.

- 119 D. W. Wang, F. Li, J. P. Zhao, W. C. Ren, Z. G. Chen, J. Tan, Z. S. Wu, I. Gentle, G. Q. Lu and H. M. Cheng, *ACS Nano*, 2009, **3**, 1745–1752.
- 120 Q. Wu, Y. X. Xu, Z. Y. Yao, A. R. Liu and G. Q. Shi, *ACS Nano*, 2010, **4**, 1963–1970.
- 121 K. Zhang, L. L. Zhang, X. S. Zhao and J. S. Wu, *Chem. Mater.*, 2010, **22**, 1392–1401.
- 122 H. L. Wang, H. S. Casalongue, Y. Y. Liang and H. J. Dai, *J. Am. Chem. Soc.*, 2010, **132**, 7472–7477.
- 123 H. J. Zheng, F. Q. Tang, Y. Jia, L. Z. Wang, Y. C. Chen, M. Lim, L. Zhang and G. Q. Lu, *Carbon*, 2009, **47**, 1534–1542.
- 124 M. F. Hassan, Z. P. Guo, Z. Chen and H. K. Liu, *J. Power Sources*, 2010, **195**, 2372–2376.
- 125 G. C. Li, C. Q. Zhang, H. R. Peng and K. Z. Chen, *Macromol. Rapid Commun.*, 2009, **30**, 1841–1845.
- 126 X. H. Huang, J. P. Tu, X. H. Xia, X. L. Wang and J. Y. Xiang, *Electrochem. Commun.*, 2008, **10**, 1288–1290.
- 127 H. J. Zheng, F. Q. Tang, M. Lim, T. Rufford, A. Mukherji, L. Z. Wang and G. Q. Lu, *J. Power Sources*, 2009, **193**, 930–934.
- 128 D. Ahn, Y. M. Koo, M. G. Kim, N. Shin, J. Park, J. Eom, J. Cho and T. J. Shin, *J. Phys. Chem. C*, 2010, **114**, 3675–3680.
- 129 J. M. Miller and B. Dunn, *Langmuir*, 1999, **15**, 799–806.
- 130 A. E. Fischer, K. A. Pettigrew, D. R. Rolison, R. M. Stroud and J. W. Long, *Nano Lett.*, 2007, **7**, 281–286.
- 131 J. W. Long, C. P. Rhodes, A. L. Young and D. R. Rolison, *Nano Lett.*, 2003, **3**, 1155–1161.
- 132 J. W. Long and D. R. Rolison, *Acc. Chem. Res.*, 2007, **40**, 854–862.
- 133 J. W. Long, M. B. Sassin, A. E. Fischer, D. R. Rolison, A. N. Mansour, V. S. Johnson, P. E. Stallworth and S. G. Greenbaum, *J. Phys. Chem. C*, 2009, **113**, 17595–17598.
- 134 C. M. Doherty, R. A. Caruso, B. M. Smarsly, P. Adelhelm and C. J. Drummond, *Chem. Mater.*, 2009, **21**, 5300–5306.
- 135 X. L. Ji, K. T. Lee and L. F. Nazar, *Nat. Mater.*, 2009, **8**, 500–506.
- 136 J. Fan, T. Wang, C. Z. Yu, B. Tu, Z. Y. Jiang and D. Y. Zhao, *Adv. Mater.*, 2004, **16**, 1432–1436.
- 137 Y. G. Wang, H. Q. Li and Y. Y. Xia, *Adv. Mater.*, 2006, **18**, 2619–2623.
- 138 I. Grigoriantis, L. Sominski, H. L. Li, I. Ifargan, D. Aurbach and A. Gedanken, *Chem. Commun.*, 2005, 921–923.
- 139 H. Kim and J. Cho, *Nano Lett.*, 2008, **8**, 3688–3691.
- 140 Y. Yang, M. T. McDowell, A. Jackson, J. J. Cha, S. S. Hong and Y. Cui, *Nano Lett.*, 2010, **10**, 1486–1491.
- 141 K. T. Lee, J. C. Lytle, N. S. Ergang, S. M. Oh and A. Stein, *Adv. Funct. Mater.*, 2005, **15**, 547–556.
- 142 L. L. Zhang, S. Li, J. T. Zhang, P. Z. Guo, J. T. Zheng and X. S. Zhao, *Chem. Mater.*, 2010, **22**, 1195–1202.
- 143 A. Magasinski, P. Dixon, B. Hertzberg, A. Kvitt, J. Ayala and G. Yushin, *Nat. Mater.*, 2010, **9**, 353–358.
- 144 D. W. Wang, F. Li, M. Liu, G. Q. Lu and H. M. Cheng, *Angew. Chem., Int. Ed.*, 2008, **47**, 373–376.
- 145 D. W. Wang, F. Li, M. Liu, G. Q. Lu and H. M. Cheng, *Angew. Chem., Int. Ed.*, 2009, **48**, 1525–1525.
- 146 Y. S. Hu, Y. G. Guo, R. Dominko, M. Gaberscek, J. Jamnik and J. Maier, *Adv. Mater.*, 2007, **19**, 1963–1966.
- 147 Y. G. Guo, Y. S. Hu, W. Sigle and J. Maier, *Adv. Mater.*, 2007, **19**, 2087–2091.
- 148 Z. Chen, Y. C. Qin, D. Weng, Q. F. Xiao, Y. T. Peng, X. L. Wang, H. X. Li, F. Wei and Y. F. Lu, *Adv. Funct. Mater.*, 2009, **19**, 3420–3426.
- 149 A. Esmanski and G. A. Ozin, *Adv. Funct. Mater.*, 2009, **19**, 1999–2010.
- 150 D. Tonti, M. J. Torralvo, E. Enciso, I. Sobrados and J. Sanz, *Chem. Mater.*, 2008, **20**, 4783–4790.
- 151 Z. Y. Wang, F. Li, N. S. Ergang and A. Stein, *Chem. Mater.*, 2006, **18**, 5543–5553.